RADC-TR-82-326
In-House Report
December 1982

FURTHER CONSIDERATIONS IN MODELS OF ROUGH SURFACE SCATTERING

Robert J. Papa
John F. Lennon
Richard L. Taylor

JUL 2 0 1983

A

ROME AIR DEVELOPMENT CENTER
Air Force Systems Command
Griffiss Air Force Base, NY 13441

20000802022

83 07 20 13
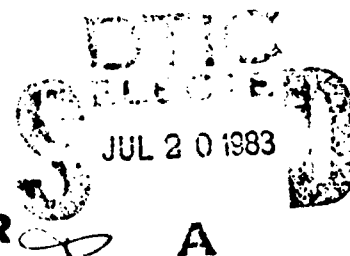
This report has been reviewed by the RADC Public Affairs Office (PA) and is releasable to the National Technical Information Service (NTIS). At NTIS it will be releasable to the general public, including foreign nations.
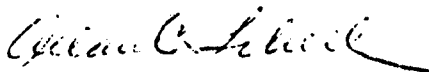
RADC-TR-82-326 has been reviewed and is approved for publication.

APPROVED: *[signature]*
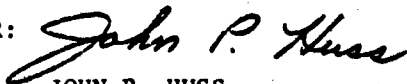
PHILIPP BLACKSMITH
Chief, EM Techniques Branch
Electromagnetic Sciences Division

APPROVED: *[signature]*

ALLAN C. SCHELL
Chief, Electromagnetic Sciences Division

FOR THE COMMANDER: *[signature]*

JOHN P. HUSS
Acting Chief, Plans Office

REPORT DOCUMENTATION PAGE	READ INSTRUCTIONS BEFORE COMPLETING FORM
1. REPORT NUMBER RADC-TR-82-326	2. GOVT ACCESSION NO. *A130424* 3. RECIPIENT'S CATALOG NUMBER
4. TITLE (and Subtitle) FURTHER CONSIDERATIONS IN MODELS OF ROUGH SURFACE SCATTERING	5. TYPE OF REPORT & PERIOD COVERED In-House
	6. PERFORMING ORG. REPORT NUMBER
7. AUTHOR(s) Robert J. Papa John F. Lennon Richard L. Taylor	8. CONTRACT OR GRANT NUMBER(s)
9. PERFORMING ORGANIZATION NAME AND ADDRESS Rome Air Development Center (EECT) Hanscom AFB Massachusetts 01731	10. PROGRAM ELEMENT PROJECT TASK AREA & WORK UNIT NUMBERS 61102F 2305J407
11. CONTROLLING OFFICE NAME AND ADDRESS Rome Air Development Center (EECT) Hanscom AFB Massachusetts 01731	12. REPORT DATE 4 November 1982
	13. NUMBER OF PAGES 69
14. MONITORING AGENCY NAME & ADDRESS (if different from Controlling Office)	15. SECURITY CLASS. (of this report) Unclassified
	15a. DECLASSIFICATION DOWNGRADING SCHEDULE

16. DISTRIBUTION STATEMENT (of this Report)

Approved for public release; distribution unlimited.

17. DISTRIBUTION STATEMENT (of the abstract entered in Block 20, if different from Report)

18. SUPPLEMENTARY NOTES

RADC Project Engineer: Robert J. Papa, RADC/EEC

19. KEY WORDS (Continue on reverse side if necessary and identify by block number)

Rough surface scattering
Electromagnetics
Glistening surface
Radar multipath

20. ABSTRACT (Continue on reverse side if necessary and identify by block number)

Several models have been developed to calculate the coherent (specular plus direct) and incoherent multipath power reaching a monopulse receiver from a beacon located over rough terrain. These models are based upon physical optics and include both Gaussian and exponential statistical distributions in surface heights. The theoretical models relate statistical parameters describing the surface to the normalized scattering cross section σ^0 of the surface. This report is concerned with three topics, in each of which

DD FORM 1473 EDITION OF 1 NOV 65 IS OBSOLETE

20. Abstract (Contd)

characteristics of the scattering from the surface depend on the degree of roughness. The first is the changes in form of the mathematical representation for σ° as the degree of roughness is varied. The next topic is concerned with alternative definitions of the glistening surface (the part of the rough surface from which diffuse power is scattered into the receiver). It is shown that, for some parameter ranges, the usual definition of glistening surface as given by Beckmann and Spizzichino is not adequate. In the final topic, the effect of the moisture content of the soil on surface scattering as a function of roughness is discussed. A wide range of results is presented in each of these areas. The implications of these findings for the prediction of system performance are discussed.

normalized scattering cross section

Contents

3

Contents

Illustrations

Tables

Further Considerations in Models of Rough Surface Scattering

1. INTRODUCTION

The scattering of electromagnetic signals from rough terrain depends on the characteristics of the surface. The scattering surface can be defined in terms of the statistical distribution of the heights, their degree of correlation, the variance of the heights, σ^2, and the complex dielectric constant appropriate to the type of terrain. Theoretical models describing rough surface[1-5] scattering relate these parameters to the normalized cross section of the terrain. This report is concerned with several factors that can affect the description of these relationships.

---

1. Beckmann, P., and Spizzichino, A. (1963) The Scattering of Electromagnetic Waves From Rough Surfaces, Macmillan Co., New York.

2. Ruck, G. T., Barrick, D. E., Stuart, W. D., and Krichbaum, C. K. (1970) Radar Cross Section Handbook, Vol. 2, Plenum Press, New York.

3. Long, N. W. (1975) Radar Reflectivity of Land and Sea, Lexington Books, Lexington, Mass.

4. Brown, G. S. (19--) A stochastic Fourier Transform approach to scattering from perfectly conducting randomly rough surfaces, IEEE Trans. Antennas Propag. (to be published).

5. Peake, W. H. (1959) The Interaction of Electromagnetic Waves With Some Natural Surfaces, Antenna Laboratory, Ohio State University Report-898-2.

1.1 Background

At RADC/EEC there is a continuing interest in improved modeling of the scattering from rough surfaces. The investigations concentrate on two main themes: the description of the surface and the electromagnetic interaction. The range of models can be seen by the descriptions in earlier reporting.[6-8] The details of the models will be presented in later sections and in the appendices. It should just be noted here that the models are comprehensive and have the capability of calculating the coherent (specular plus direct) and incoherent multipath power reaching a monopulse receiver from a beacon located over rough terrain. Discussions of coherence and the methods for calculating the coherent and incoherent power are given in the appendices. One additional point is that in these models we use the concept of "glistening surface" (for a given set of antenna positions, that part of the rough surface that reflects a significant amount of the transmitted energy into the receiver) as described by Beckmann and Spizzichino.[1] A geometrical representation of the scattering from the surface is shown in Figure 1.
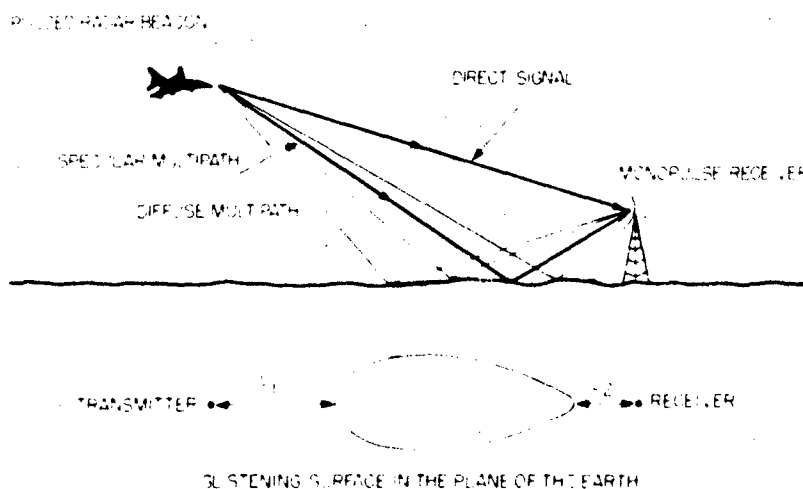
Figure 1. Geometrical Representation of the Scattering From Rough Surfaces

6. Papa, R.J., and Lennon, J.F. (1980) Electromagnetic scattering from rough surfaces based on statistical characterization of the terrain, International Radio Science Symposium, (URSI), June 1980), Quebec, Canada.

7. Papa, R.J., Lennon, J.F., and Taylor, R.L. (1980) Electromagnetic Wave Scattering From Rough Terrain, RADC-TR-80-300, AD-A-09839.

8. Papa, R.J., Lennon, J.F., and Taylor, R.L. (1982) The Need For An Expanded Definition of Glistening Surface, RADC-TR-82-271.

1.2 Scope

In this report we will be addressing three different topics related to the scattering from rough surfaces and will show how all of them are sensitive to the actual degree of roughness. The first is the determination of the form for the normalized cross section of the surface, σ°. The usual form is based on physical optics and the asymptotic evaluation of integrals representing σ° in the limit of very rough surfaces for bivariate Gaussian and exponential surface-height distributions. In the exponential case the uncorrelated variates are not independent and, for intermediate levels of roughness, this leads to a form for σ° different from the usual result. The next topic is that of the glistening surface. For some parameter ranges, the classical definition of the glistening surface as given by Beckmann and Spizzichino is not adequate. Their definition does not account for the angular dependence of the scattering matrix in the expression for σ° (the normalized cross section of the rough surface). In addition, it may suppress contributions from areas close to the antennas. The final roughness dependent effect discussed here is how the scattering from a given type of surface is effected by the amount of moisture present in the soil. To represent this, the dielectric constant of the surface, for a range of conditions, is chosen to correspond to arid, normal, and very wet soil. The effect is again sensitive to the degree of roughness.

The results of this study can have implications for the estimation of radar system performance. Two aspects are important. First, there is the question of establishing system design criteria that are cost effective. Second, the assessment of system performance variability is related to the discussions of the effect of surface roughness on moisture dependent scattering.

2. THE NORMALIZED CROSS SECTION OF RANDOM ROUGH SURFACES

In this section we will discuss the basic theoretical considerations involved in the determination of the rough surface scattering cross-section. Particular consideration will be given to limitations of the theories and the effects of the statistical properties assumed to describe the surface height distribution of the scattering area.

2.1 Single-Scale-of-Roughness Theories

Two major theoretical formulations for the normalized cross section, the physical optics model and the perturbation theory model, will be considered including the delineation of conditions under which each applies.

2.1.1 PHYSICAL OPTICS

In the physical optics approximation,[1,2] the radius of curvature of the irregularities is assumed to be large compared to a wavelength ($R_c \gg \lambda$). The recent work by Brown[4] has shown that this condition is not, in itself, sufficient for physical optics to be applicable. An additional constraint is required, such as the surface slopes must also be small ($T \gg \sigma$), where T = surface correlation length and σ = standard deviation in surface height. Also, the total field on the rough surface may be expressed as the sum of the incident field plus the scattered field. Because the radii of curvature are assumed to be large compared to a wavelength, the scattered field is expressed as the incident field multiplied by the Fresnel plane wave reflection coefficient. Then, the normalized scattering cross section (σ°) for the surface is derived by substituting this approximation for the total field on the surface into the Kirchhoff integral (scalar or vector form) expression for the scattered field. The expression that is derived for the normalized cross section σ° of the rough surface depends upon the probability distribution function (PDF) of the surface heights, the surface correlation function, standard deviation in surface height, surface correlation length, and complex dielectric constant of the surface.

2.1.2 PERTURBATION THEORY

The second conventional method for deriving an expression for σ° with a single scale of surface roughness is the Rayleigh-Rice or perturbation method. Here, it is assumed that the scattered or transmitted fields from or across a rough surface can be represented by a superposition of plane waves propagating away from the boundary with unknown amplitudes (Rice,[9] Peake,[5] and Ruck et al[2]). Also, it is assumed that the standard deviation in surface height is small compared to a wavelength and that the surface slopes are small. Then, the scattered fields are expanded in a perturbation series. The unknown scattered-field amplitudes are determined by requiring each order of perturbation to satisfy Maxwell's equations and the boundary conditions. The expression that is derived for σ° is proportional to the surface height spectral density, the fourth power of the wavenumber, and the fourth power of the surface-height standard deviation.

2.2 Multiple Scales of Roughness

There have been several models developed to describe wave scattering from a surface with two or more scales of roughness. Some two-scale models have been

---

9. Rice, S.D. (1951) Reflection of electromagnetic waves by slightly rough surfaces, The Theory of Electromagnetic Waves, M. Kline, Ed., Wiley, New York.

derived by assuming that the small scale of roughness obeys the criteria for the perturbation solution that is superimposed on a large scale of roughness that obeys the physical optics criterion (Wright[10] and Fuks[11]). Brown[12] has obtained an expression for σ° with two scales of roughness using a perturbation technique first derived by Burroughs.[13] Bahar[14] has used the full wave approach to derive expressions for σ° to describe the scattering of em waves from a rough surface with more than one scale of roughness. The solutions have been shown to reduce to the physical optics result or the perturbation result in appropriate limits.

2.3 Surface Height Statistic

2.3.1 GAUSSIAN HEIGHT VARIATES

Most authors have considered that the random rough surface from which the scattering occurs is Gaussian in nature. There are two main reasons for this assumption. In the first case, there are a number of instances in which agreement with experiment has been obtained with this assumption. Secondly, this assumption is attractive because of the statistical properties of Gaussian distributions. For instance, sums of Gaussian variates are also Gaussian. Another example of perhaps more interest is the property that once the variates become uncorrelated, their respective marginal densities are independent. Both of these aspects are important in the mathematical analyses for the scattering cross section of the surface.

2.3.2 NON-GAUSSIAN INDEPENDENT VARIATES

The first serious effort to investigate em-wave scattering from non-Gaussian rough surfaces is presented in the report by Barrick.[15] Here, expressions for σ° are derived under the assumptions of physical optics for a modified Bessel joint PDF and a Gaussian joint PDF. Both a Gaussian and an exponential function are

10. Wright, J.W. (1966) Backscattering from capillary waves with application to sea clutter, IEEE Trans. Antennas Propag. AP-14:749.

11. Fuks, I.M. (1966) Contribution to the theory of radio wave scattering on the perturbed sea surface, Izvestia Vyshikh Uchebnykh Zavedenii Radiofizika 5:876.

12. Brown, G.S. (1978) Backscattering from a Gaussian distributed perfectly conducting rough surface, IEEE Trans. Antennas Propag. AP-26:472.

13. Burrows, M.L. (1967) A reformulated boundary perturbation theory in electromagnetism and its application to a sphere. Can. J. Phys. 45:1729.

14. Bahar, E. (1981) Scattering cross sections for random rough surfaces: Full wave analysis, Radio Sci. 16:331-341.

15. Barrick, D.F. (1965) A More Exact Theory of Backscattering From Statistically Rough Surfaces, Ohio State University Research Foundation, Report 1388-18.

assumed for the surface-height correlation function. Beckmann has used a form for the modified Bessel joint PDF that was first proposed by Ott.[16] If Z_1 and Z_2 represent surface heights at two distinct points on the surface, then the modified Bessel-joint PDF is given by

$$p_B(Z_1, Z_2) = \left(\frac{9}{\pi^2 \sigma^4 (1 - c^2)} \right) |Z_2| |Z_1 - cZ_2| K_1 \left[\frac{\sqrt{3} |Z_1 - cZ_2|}{\sigma(1 - c^2)^{1/2}} \right] K_1 \left[\frac{\sqrt{3} |Z_2|}{\sigma} \right] ,$$

where σ is the standard deviation in surface height, c is the correlation function, and K_1 is the modified Bessel function of the first kind of order one. It should be noted that when $\tau = \sqrt{(x_1 - x_2)^2 + (y_1 - y_2)^2} \to \infty$ and $c(\tau) \to 0$, then $p_B(Z_1, Z_2) = p_1(Z_1) p_2(Z_2)$. This means that decorrelation implies statistical independence for this PDF. However, the two variates are not described by identical marginal probability densities in this case and the meaning of this result is somewhat unclear.

In 1973, Beckmann[17] investigated em-wave scattering from rough non-Gaussian surfaces using the assumptions of physical optics. The method assumes that the joint PDF $p(Z_1, Z_2, c)$ can be derived from the marginal density $p(z)$ and known correlation function $c(\tau)$. The technique uses the properties of classical sets of polynomials (Hermite, generalized Laguerre, and Jacobi), which are orthogonal over some interval with respect to some weighting function. Another assumption is that the joint PDF $p(Z_1, Z_2, c) = p_1(Z_1) p_1(Z_2)$ as $c(\tau \to \infty) \to 0$, that is, decorrelation leads to statistical independence.

2.3.3 NON-GAUSSIAN DEPENDENT VARIATES

The transformation of joint surface-height probability densities into sets of uncorrelated variates does not always lead to statistical independence. In Ruck et al.,[2] Barrick introduced the bivariate exponential surface height PDF:

$$p_E(Z_1, Z_2) = \left(\frac{3}{2\pi\sigma^2 (1 - c^2)^{1/2}} \right) \exp \left[- \left(\frac{Z_1^2 - 2cZ_1 Z_2 + Z_2^2}{(1/3)\sigma^2 (1 - c^2)} \right)^{1/2} \right] .$$

The uncorrelated result for this case is not a pair of independent variates, and this leads to complications in the theoretical development of σ°. The authors have

---

16. Ott, R.H. (1967) A Theoretical Model for Scattering From Rough Surfaces With Applications to the Moon and Sea, Ohio State University Research Foundation, Report-1388-1.

17. Beckmann, P. (1973) Scattering by non-Gaussian surfaces, IEEE Trans. Antennas Propag. AP-21:169.

used variations of this distribution in several previous studies.[7,18,19] As a result of applying hypothesis testing procedures (see Appendix A) it was found that for the radar site [the Discrete Address Beacon System in Massachusetts (DABS)[20]] used for experimental comparison, the terrain heights fit better to a bivariate exponential distribution than a bivariate Gaussian distribution.

Recently, Brown[21] has considered scattering from perfectly-conducting random surfaces for which decorrelation does not imply statistical independence. By using an exact theory for the current induced on the surface and the stochastic Fourier transform approach, it is shown that the incoherent scattered power consists of two parts. The first part corresponds to what is normally termed the diffuse power, that is, the incoherent power scattered in all directions. The second part is incoherent power scattered specifically in the specular direction.

2.4 The Conditions For Physical Optics

In our opinion, the physical optics models of rough surface scattering are the most rigorous of all models to date. The analyses developed herein are based on the limits of physical optics assumptions. For the rough surface scattering case we can examine the parameters in relation to those conditions for which physical optics applies. In this analysis the rough surface heights are assumed to be related by Gaussian correlation functions.

The rough surface is given by the equation $z = \zeta(x, y)$. For an isotropic surface, the slopes $\frac{\partial z}{\partial x}$ and $\frac{\partial z}{\partial y}$ are equal. The average slope is given by

$$\overline{z'} = \left[\left| \left\langle \frac{\partial z}{\partial x} \frac{\partial z}{\partial y} \right\rangle \right| \right]^{1/2} \quad ,$$

where $\langle \ \rangle$ denotes expectation value. First, we assume that the surface autocorrelation functional is $R = \sigma^2 e^{-\tau^2/T^2}$. Here τ is again the separation between points, $\tau = \left[(x_1 - x_2)^2 + (y_1 - y_2)^2 \right]^{1/2}$. The square of the radius of curvature, R_c of a curve is given by

18. Lennon, J. F., and Papa, R.J. (1980) Statistical Characterization of Rough Terrain, RADC-TR-80-9, AD A087746.

19. Papa, R.J., Lennon, J.F., and Taylor, R.L. (1980) Prediction of Electromagnetic Scattering for Rough Terrain Using Statistical Parameters Derived From Digitized Topographic Maps, RADC-TR-80-289, AD A094104.

20. McGarty, T.P. (1975) The Statistical Characteristics of Diffuse Multipath and Its Effect on Antenna Performance, ESD-TR-75-145, AD A009869.

21. Brown, G.S. (1982) Scattering from a class of randomly rough surfaces, Radio Sci. (to be published).

$$R_c^2 = \frac{(1 + (z')^2)^3}{(z'')^2} \quad .$$

The expectation value of R_c^2 is given by

$$\left\langle R_c^2 \right\rangle = \left\langle \frac{(1 + (z')^2)^3}{(z'')^2} \right\rangle \quad .$$

To simplify the evaluation of this quantity we will approximate $\left\langle R_c^2 \right\rangle$ by the following expression:

$$\left\langle R_c^2 \right\rangle \approx \frac{\left\langle (1 + (z')^2)^3 \right\rangle}{\left\langle (z'')^2 \right\rangle} = \frac{(1 + \overline{(z')^2})^3}{\overline{(z'')^2}} \quad .$$

The average of $(z')^2$ is given by

$$\overline{(z')^2} = \left| \left\langle \frac{\partial \zeta}{\partial x} \frac{\partial \zeta}{\partial x} \right\rangle \right| = \left| \frac{\partial^2 R(\tau = 0)}{\partial \tau^2} \right|$$

and the average of $(z'')^2$ is given by

$$\overline{(z'')^2} = \left| \frac{\partial^4 R(\tau = 0)}{\partial \tau^4} \right| = \frac{12\sigma^2}{T^4} \quad .$$

Then, an approximate expression for the average radius of curvature is given by

$$\overline{R}_c \approx \frac{T^2}{\sqrt{12}\,\sigma} \left[1 + 2\sigma^2/T^2 \right]^{3/2} \quad .$$

We have already discussed the fact that one set of sufficient conditions for physical optics to apply is $R_c \gg \lambda$ and $1 \gg \sigma/T$. If we consider the equations for R_c and a new condition $T^2/\sigma \gg \lambda$ then, these relations, along with the relation $T \gg \sigma$, lead to the simpler (in the sense of being more directly seen) set of sufficient conditions for physical optics, $\sigma/T \ll 1$ and $T^2/\sigma \gg \lambda$, for a surface with a Gaussian autocorrelation function. One interesting point to note is that these conditions hold for all values of the Rayleigh roughness parameter, Σ where

14

$\Sigma = \left(\frac{2\pi}{\lambda}\right) \sigma (\cos \theta_i + \cos \theta_s)$. Here λ = em-wavelength wavelength, θ_i = angle of incidence, and θ_s angle of scattering measured with respect to surface normal.

2.5 $\sigma°$ Determination

In this chapter, comparisons will be made between the exact integral representation for $\sigma°$ and the asymptotic representation for $\sigma°$ for both exponential and Gaussian PDFs as a function of the Rayleigh parameter Σ. It will be shown that for exponentially-distributed surface heights, great care must be exercised in the use of the expression for $\sigma°$ as given in the book by Ruck et al.[2] In Appendix B, it is shown how expressions for $\sigma°$ may be derived for bivariate exponential PDFs under the assumptions of physical optics. For large Rayleigh parameter Σ, a steepest descent evaluation is made to obtain the expression for $\sigma°$ first given by Barrick in Ruck et al.[2] It will be shown in the results of this chapter that the asymptotic expression given for $\sigma°$ is not accurate unless Σ is very large. This difficulty arises because the bivariate exponential PDF does not reduce to independent variates Z_1 and Z_2 as $\tau = \left[(x_1 - x_2)^2 + (y_1 - y_2)^2 \right]^{1/2} \to \infty$, and, as Σ increases, the normalized cross section $\sigma°$ does not approach zero as rapidly as in the Gaussian PDF case.

For the purpose of this study, the behavior of $\sigma°$ is discussed in terms of the behavior of the slope-dependent statistical quantity J. This is explained in detail in Appendix B. The formulations are developed for various ranges of Σ. The restrictions and regions of agreement are assessed in the following sections.

2.5.1 DESCRIPTION OF TABULAR RESULTS

Tables 1 through 18 present values of the quantity J as a function of the azimuthal scattering angle, PHISC, for both Gaussian-distributed surface heights and exponentially-distributed surface heights. This form of presentation permits us to examine whether azimuthal displacement affects agreement. In these tables, Σ is the Rayleigh roughness parameter and T is the correlation length in meters. The values assumed by the Rayleigh parameter are given as Σ^2 = 95.864, 20.13, 10.0, 1.0, and 0.1 (for exponential surfaces). The correlation length is 5 m and 15 m.

For Gaussian-distributed surfaces, SUM refers to the summation representation for J; APPROX refers to the steepest descent evaluation of the integral representation for J (valid for $\Sigma \gg 1$); the INTEG refers to the integral representation for J. For the exponentially-distributed surfaces, APPROX refers to the steepest descent evaluation of the integral representation for J (valid for $\Sigma \gg 1$); SING INTEG refers to the integral representation for J; and POWER EXPAN refers to the evaluation of the integral representation for J obtained by expanding the denominator in a power series (valid for $\Sigma < 1$). These are all derived in Appendix B.

Table 1. Values of J-integral as a Function of Azimuthal Scattering Angle: $\Sigma^2 = 95.864$, T = 5.0, Gaussian Surface

PHISC	SUM	APPROX	INTEG
0.5	$2.605 \cdot 10^{-14}$	1009.34	1019.66
1.0	$2.07 \cdot 10^{-14}$	951.76	960.30
1.5	$1.42 \cdot 10^{-14}$	863.00	869.02
2.0	$8.31 \cdot 10^{-15}$	752.47	755.77
2.5	$4.19 \cdot 10^{-15}$	630.91	631.78
3.0	$1.81 \cdot 10^{-15}$	508.70	507.77
3.5	$6.75 \cdot 10^{-16}$	394.42	392.48

Table 2. Values of J-integral as a Function of Azimuthal Scattering Angle: $\Sigma^2 = 20.13$, T = 5.0, Gaussian Surface

PHISC	SUM	APPROX	INTEG
0.5	976.13	1009.34	1062.85
1.0	912.20	951.76	995.29
1.5	815.34	863.00	892.72
2.0	697.65	752.47	767.70
2.5	572.10	630.91	633.74
3.0	450.19	508.70	502.92
3.5	340.41	394.42	384.26

Table 3.   Values of J-integral as a Function of Azimuthal
Scattering Angle: $\Sigma^2 = 10.0$, T = 5.0, Gaussian Surface

PHISC	SUM	APPROX	INTEG
0.5	1132.86	1009.34	1131.37
1.0	1048.11	951.76	1049.21
1.5	924.33	863.00	924.153
2.0	780.01	752.47	779.72
2.5	632.06	630.91	632.31
3.0	493.38	508.70	493.41
3.5	372.81	394.42	371.93

Table 4.   Values of J-integral as a Function of Azimuthal
Scattering Angle: $\Sigma^2 = 1.0$, T = 5.0, Gaussian Surface

PHISC	SUM	APPROX	INTEG
0.5	490.62	1009.34	6572.226
1.0	466.26	951.76	-950.11
1.5	428.49	863.00	677.40
2.0	381.06	752.47	582 43
2.5	328.25	630.91	-74.32
3.0	274.28	508.70	765.26
3.5	222.70	394.42	-296.66

17

Table 5. Values of J-integral as a Function of Azimuthal Scattering Angle: $\Sigma^2 = 95.864$, T = 15.0, Gaussian Surface

PHISC	SUM	APPROX	INTEG
0.5	$1.27 \cdot 10^{-13}$	7752.62	7806.46
1.0	$1.62 \cdot 10^{-14}$	4569.19	4560.75
1.5	$5.30 \cdot 10^{-16}$	1893.11	1875.07
2.0	$4.47 \cdot 10^{-18}$	551.43	547.80
2.5	$9.78 \cdot 10^{-21}$	112.93	115.15
3.0	$5.57 \cdot 10^{-24}$	16.26	17.66
3.5	$8.29 \cdot 10^{-28}$	1.65	2.01

Table 6. Values of J-integral as a Function of Azimuthal Scattering Angle: $\Sigma^2 = 20.13$, T = 15.0, Gaussian Surface

PHISC	SUM	APPROX	INTEG
0.5	7322.55	7752.62	8018.06
1.0	4042.85	4569.19	4516.70
1.5	1558.37	1893.12	1808.72
2.0	434.20	551.43	537.02
2.5	89.99	112.93	122.95
3.0	14.15	16.26	22.44
3.5	1.71	1.65	3.36

Table 7. Values of J-integral as a Function of Azimuthal Scattering Angle: $\Sigma^2 = 10.0$, T = 15.0, Gaussian Surface

PHISC	SUM	APPROX	INTEG
0.5	8299.55	7752.62	8298.12
1.0	4430.46	4569.19	4431.60
1.5	1731.12	1893.12	1730.97
2.0	523.01	551.43	527.73
2.5	131.64	112.93	131.90
3.0	27.74	16.26	27.77
3.5	5.06	1.65	4.90

Table 8. Values of J-integral as a Function of Azimuthal Scattering Angle: $\Sigma^2 = 1.0$, T = 15.0, Gaussian Surface

PHISC	SUM	APPROX	INTEG
0.5	3850.28	7752.62	9931.88
1.0	2464.43	4569.19	1048.07
1.5	1221.87	1893.12	1470.77
2.0	506.02	551.43	707.39
2.5	193.80	112.93	-208.77
3.0	73.71	16.26	564.70
3.5	27.95	1.65	-491.41

Table 9. Values of J-integral as a Function of Azimuthal Scattering Angle: $\Sigma^2 = 95.864$, $T = 5.0$, Exponential Surface

PHISC	APPROX	SING INTEG
0.5	2188	2231
1.0	1554	1555
1.5	1104	1099
2.0	784	779
2.5	556	553
3.0	395	393
3.5	280	279

Table 10. Values of J-integral as a Function of Azimuthal Scattering Angle: $\Sigma^2 = 29.13$, $T = 5.0$, Exponential Surface

PHISC	APPROX	SING INTEG
0.5	2188	2143
1.0	1555	1550
1.5	1104	1081
2.0	784	768
2.5	556	541
3.0	395	384
3.5	280	274

20

Table 11. Values of J-integral as a Function of Azimuthal Scattering Angle: $\Sigma^2 = 10.0$, T = 5.0, Exponential Surface

PHISC	APPROX	SING INTEG
0.5	2188	2395
1.0	1555	1522
1.5	1104	1084
2.0	784	769
2.5	556	526
3.0	395	384
3.5	280	269

Table 12. Values of J-integral as a Function of Azimuthal Scattering Angle: $\Sigma^2 = 1.0$, T = 5.0, Exponential Surface

PHISC	APPROX	SING INTEG	POWER EXPAN
0.5	2188	1078	1009
1.0	1555	3£9	952
1.5	1104	398	863
2.0	784	320	752
2.5	556	273	631
3.0	395	234	509
3.5	280	182	394

Table 13. Values of J-integral as a Function of Azimuthal Scattering Angle: $\Sigma^2 = 0.1$, T = 5.0, Exponential Surface

PHISC	APPROX	SING INTEG	POWER EXPAN
0.5	2188	14	10
1.0	1555	13	10
1.5	1103	11	10
2.0	784	10	10
2.5	556	9	10
3.0	395	9	10
3.5	280	8	9

Table 14. Values of J-integral as a Function of Azimuthal Scattering Angle: $\Sigma^2 = 95.864$, T = 15.0, Exponential Surface

PHISC	APPROX	SING INTEG
0.5	9881	9850
1.0	3544	3525
1.5	1269	1264
2.0	454	454
2.5	162	163
3.0	58	58
3.5	21	21

22

Table 15. Values of J-integral as a Function of
Azimuthal Scattering Angle: $\Sigma^2 = 20.13$, $T = 15.0$,
Exponential Surface

PHISC	APPROX	SING INTEG
0.5	9881	9676
1.0	3544	3450
1.5	1269	1247
2.0	454	453
2.5	162	165
3.0	58	60
3.5	21	22

Table 16. Values of J-integral as a Function of
Azimuthal Scattering Angle: $\Sigma^2 = 10.0$, $T = 15.0$,
Exponential Surface

PHISC	APPROX	SING INTEG
0.5	9881	9985
1.0	3544	3401
1.5	1269	1251
2.0	454	476
2.5	162	167
3.0	58	71
3.5	21	24

Table 17. Values of J-integral as a Function of Azimuthal Scattering Angle: $\Sigma^2 = 1.0$, T = 15.0, Exponential Surface

PHISC	APPROX	SING INTEG	POWER EXPAN
0.5	9881	3735	7753
1.0	3544	1997	4569
1.5	1269	1071	1393
2.0	454	464	551
2.5	162	200	113
3.0	58	96	16
3.5	21	38	2

Table 18. Values of J-integral as a Function of Azimuthal Scattering Angle: $\Sigma^2 = 0.1$, T = 15.0, Exponential Surface

PHISC	APPROX	SING INTEG	POWER EXPAN
0.5	9881	85	91
1.0	3544	80	86
1.5	1269	73	79
2.0	454	64	70
2.5	162	54	60
3.0	58	44	49
3.5	21	35	39

2.5.2 GAUSSIAN RESULTS

Examination of Tables 1 through 8 shows that the SUM representation for J (Gaussian surface) is very poor for $\Sigma \gg 1$ and becomes more and more accurate as Σ decreases. For $\Sigma \gg 1$, the asymptotic expression APPROX and the integral representation for J agree to within 1 percent for all PHISC. As Σ decreases, the asymptotic representation and the integral representation disagree more and more with each other. Finally at $\Sigma = 1$, the asymptotic representation is very inaccurate, and so is the integral representation because of numerical inaccuracies in evaluating INTEG. The problem here is that as Σ decreases, the decay of the integrand as τ increases is slow, and there are many oscillations of the integrand (see Appendix B). At $\Sigma = 1$, and $\Sigma < 1$, the SUM representation of J is the only accurate representation.

2.5.3 EXPONENTIAL RESULTS

A study of Tables 11 through 18 reveals several facts about the behavior of J (and hence σ°) for exponentially-distributed surfaces. For large Rayleigh parameters $\Sigma \gg 1$, the asymptotic evaluation of the integral for J, APPROX and the integral representation for J, SING INTEG agree to within 1 percent for all azimuthal scattering angles, PHISC. As Σ decreases, APPROX and SING INTEG disagree more and more with each other until at $\Sigma = 1$, the asymptotic representation is very inaccurate. As opposed to the Gaussian case, for the exponentially-distributed surface, the integral representation for J is accurate for all values of the Rayleigh parameter. At $\Sigma = 1$, the asymptotic representation is not accurate, whereas there is better agreement between the integral representation and the power-series expansion representation. For $\Sigma = 0.1$, the asymptotic representation is extremely inaccurate, but there is very good agreement between the integral representation and the power-series expansion representation.

2.5.4 SUMMARY OF RESULTS

To summarize, for the Gaussian-distributed surface heights, the asymptotic representation and the integral representation for J are accurate for large Rayleigh parameters $\Sigma \gg 1$. For intermediate Rayleigh parameters, the sum representation and the integral representation are accurate. For small Rayleigh parameters $\Sigma < 1$, the series representation is the only representation that is accurate. On the other hand, for the exponentially-distributed surface heights, the integral representation for J is accurate for all Rayleigh parameters. The asymptotic representation is accurate for large Rayleigh parameter and starts to deviate from the integral representation for intermediate Rayleigh parameters. For small Rayleigh parameters, the power-series expansion representation is accurate.

25

3. COMPARISON OF RESULTS BETWEEN STANDARD GLISTENING SURFACE AND EXTENDED GLISTENING SURFACE

In a previous report,[8] an analysis was made of the conditions under which the conventional definition of length of the glistening surface, as given by Beckmann and Spizzichino[1] (see Appendix C), is not valid. It was shown that, for a wide range of conditions, significant amounts of incoherent scattered power can be received from areas beyond the conventional length of the glistening surface. The amount of additional incoherent power not included under the conventional definition depends on the ratio σ/T, except for the case where both transmitter and receiver are very close to the surface. It was shown that the trends in the behavior of the glistening surface are similar for vertical or horizontal polarization, Gaussian- or exponential-surface height distributions, and for different signal frequencies in the S-band to L-band region. These previous investigations[8] examined the effects of extending the length of the glistening surface, while the Beckmann and Spizzichino[1] definition of glistening surface width (W) was used (see Appendices A and C). The diffuse scattered power contribution from each increment of length (Δl) along the glistening surface is obtained by multiplying the product of the centerline value of σ° ($\phi_s = 0$), W, and Δl by the appropriate azimuthal and elevation plane antenna power-pattern distributions (here, ϕ_s = azimuthal scattering angle).

In this report, the effects of extending both the length and width of the glistening surface will be examined. As explained in Appendix C, the length is extended by integrating the product of σ° with the corresponding elevation and azimuthal receiver and transmitter gain functions over the entire distance between the two antennas. The width of the glistening surface is extended by integrating the azimuthally dependent cross section σ° out to the point where the azimuthal antenna pattern has dropped to about -45 dB (average sidelobe level) of the peak. Two different azimuthal power patterns of the receiver are considered in these investigations: a monopulse difference pattern (shown in Figure 2) and a power pattern that has no null at boresight ($\phi_s = 0.0$). This second power pattern is similar to the original monopulse difference pattern, except that the peak at about $\pm 3^\circ$ remains constant over the azimuthal angle range $-3^\circ \le \phi_s \le 3^\circ$.

Figures 3 and 4 show the diffusely scattered power (in Watts) as a function of range (in nmi and km) for the monopulse receiving antenna. The rough surface is uniform with a correlation length T = 100 m and three variances in surface height: $\sigma^2 = 1 \text{ m}^2$, 10 m^2, and 100 m^2. The em wavelength $\lambda = 0.275$ m and the complex dielectric constant of the surface $\epsilon_r = 80 + j9.0$.

Figure 3 is a triple plot of diffuse power (P_{DIFF}) vs range between transmitter and receiver where the Beckmann and Spizzichino[1] definition of glistening

26
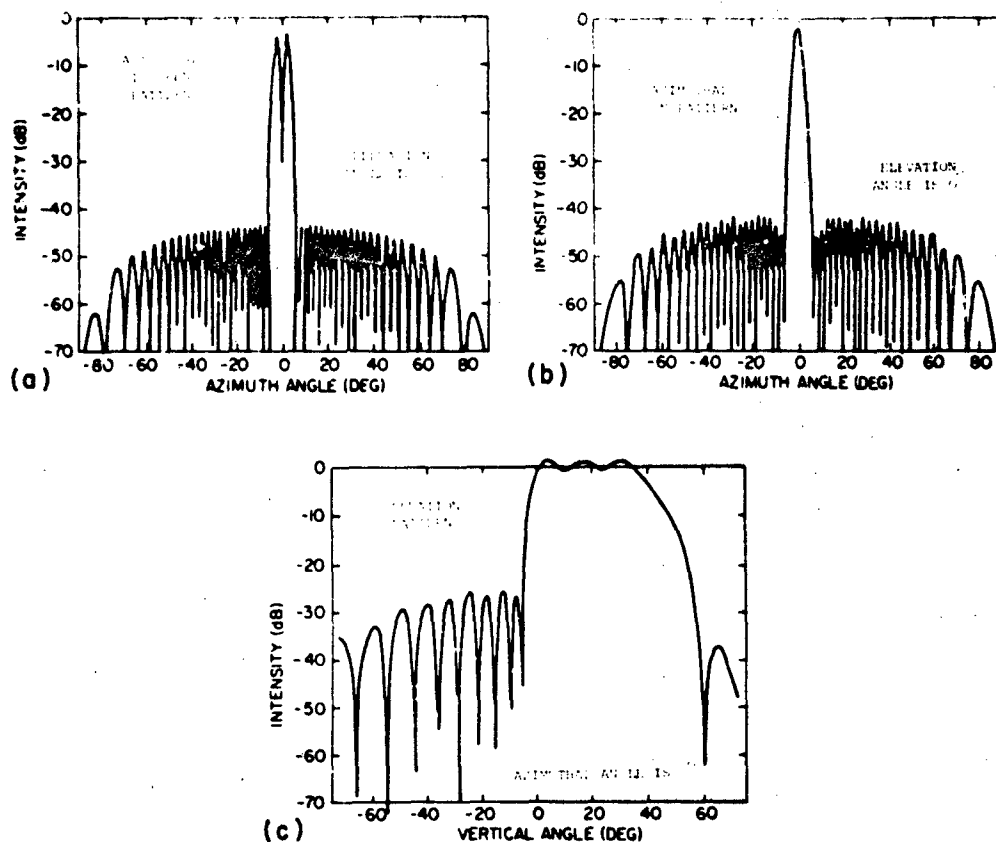
Figure 2. Azimuthal Difference and Azimuthal Sum Pattern and Elevation Pattern of DABS Antenna

surface length and width was used. It may be noted from this figure that the cut-off in P_{DIFF} at short ranges for $\sigma^2 = 1$ m^2 and $\sigma^2 = 10$ m^2 disappears as the variance increases to $\sigma^2 = 100$ m^2. The cutoffs in P_{DIFF} at short ranges is due to the vanishing of the glistening surface according to the Beckmann and Spizzichino[1] definition. In Figure 4, the extended length and width definition of glistening surface was used to calculate P_{DIFF} vs. range. It may be noted that extending the length and width of the glistening surface removes the cutoffs in P_{DIFF} vs range, so that the glistening surface exists at all ranges for all values of the variance σ^2. Also, comparing Figure 3 with Figure 4, it may be noted that for $\sigma^2 = 10$ m^2 and $\sigma^2 = 100$ m^2, extending the length and width of the glistening surface causes an increase in P_{DIFF} for all ranges. On the other hand, for $\sigma^2 = 1$ m^2, P_{DIFF} for the extended definition is greater than P_{DIFF} for the standard definition only for

27

Figure 3. Diffuse Power Behavior for Azimuthal Difference Power Pattern; Standard Glistening Surface, $T = 100$ m, $\sigma^2 = 1,\ 10,\ 100\ \text{m}^2$

Figure 4. Diffuse Power Behavior for Azimuthal Difference Power Pattern; Full Integration, $T = 100$ m, $\sigma^2 = 1,\ 10,\ 100\ \text{m}^2$

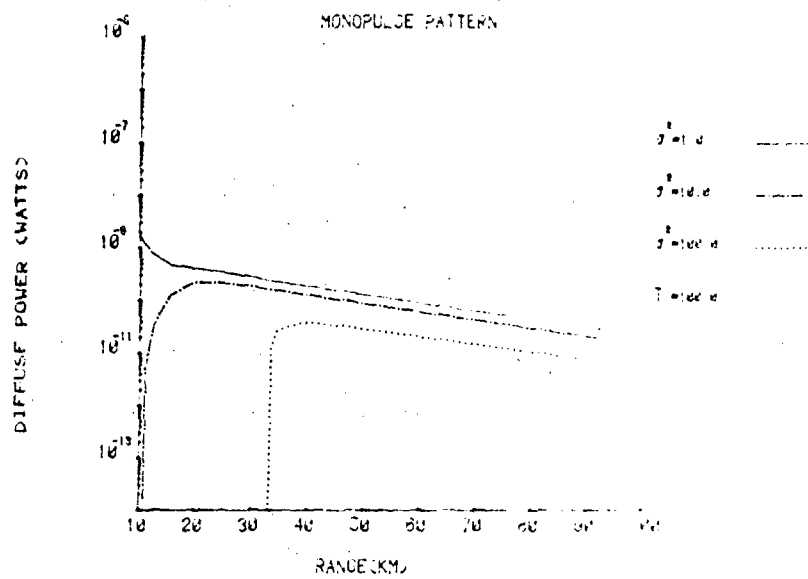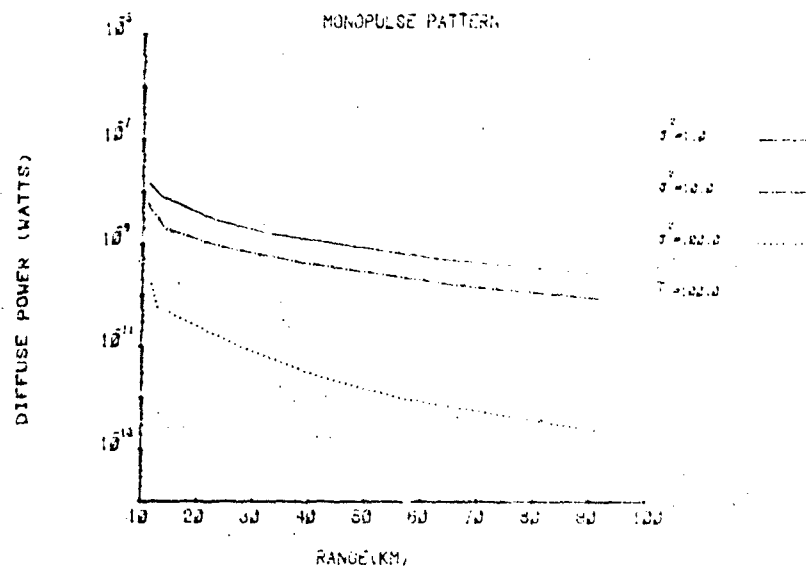short ranges. For long ranges, $\sigma^2 = 1 \text{ m}^2$ results in a sharp dropoff of σ^* with increasing azimuthal angle ϕ_s, so that P_{DIFF} for the extended definition is less than P_{DIFF} for the standard definition (which, as described in Appendix C, is obtained by multiplying σ° ($\phi_s = 0$) by the classical width of the glistening surface).

All the parameters in Figures 5 and 6 are the same as in Figures 3 and 4, except for the receiving antenna pattern that is now centrally uniform. Figure 5 corresponds to the standard definition of glistening surface and Figure 6 corresponds to the extended length and width definition. By making comparisons between these four figures, it may be noted that the differences in P_{DIFF} between the extended definition and the standard definition are, in general, the same for the modified antenna pattern as for the monopulse pattern. There is the disappearance of the cutoffs at short ranges for $\sigma^2 = 1 \text{ m}^2$ and $\sigma^2 = 10 \text{ m}^2$, and there is always an increase in P_{DIFF} when the glistening surface is extended. The one notable difference is that for the modified antenna pattern, extending the glistening surface causes P_{DIFF} to increase at long ranges for $\sigma^2 = 1 \text{ m}^2$. For the original monopulse pattern, P_{DIFF} decreased as the glistening surface was extended. This difference in behavior may be attributed to the fact that removing the null at boresight in the receiving pattern causes an increase in P_{DIFF} (because σ° is a maximum at $\phi_s = 0^\circ$), which compensates for the falloff in σ° as ϕ_s increases.

To conclude this section we will compare the results of the two models with data taken at the DABS site by Lincoln Laboratory personnel. This data consisted of the coherent power in the sum channel and the boresight angular uncertainty in the difference channel of a monopulse receiver located on the ground. The transmitter was located on an aircraft. The data consisting of monopulse boresight angular uncertainty vs range was processed by removing the bias in boresight pointing error due to electrical imbalances in the system and then converting the azimuthal angular uncertainty into an equivalent diffuse power using the equations and system parameters given in Appendix A. The crosses in Figure 7 show the results of the processed DABS data.

In Appendix A, and in previous work[6, 7, 8, 18, 19] it was discussed how statistical estimation theory was applied to digitized terrain maps to determine parameters that may be used in the em scattering models. The techniques were applied to terrain at an eastern Massachusetts site (DABS). A data base of topographic elevations for this area is available at the Electromagnetic Compatibility Analysis Center (ECAC) in Annapolis, Md. This was prepared from digitized terrain maps supplied by the Defense Mapping Agency (DMA). The area of interest is divided into rectangular cells, each with sides about 2 km. The statistical analysis is then applied to the individual cells.
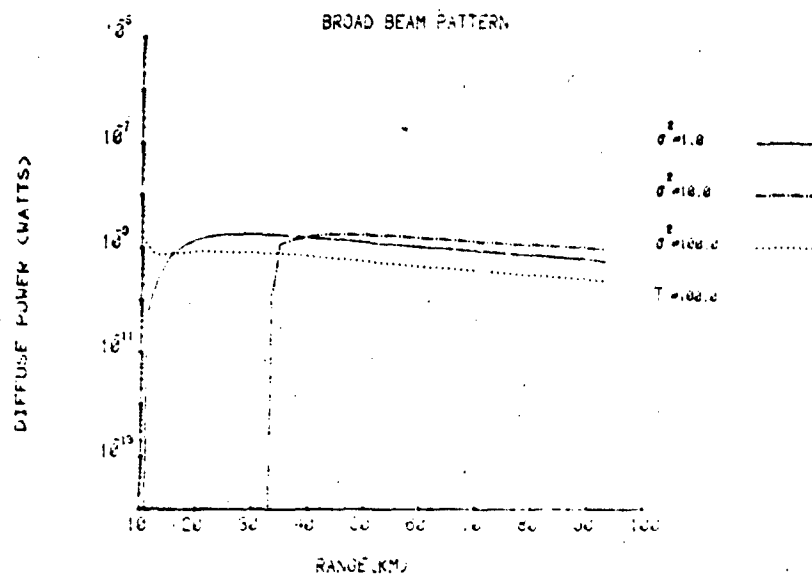
Figure 5. Diffuse Power Behavior for a Centrally-uniform Power Pattern; Full Integration, $T = 100$ m, $\sigma^2 = 1, 10, 100$ m^2
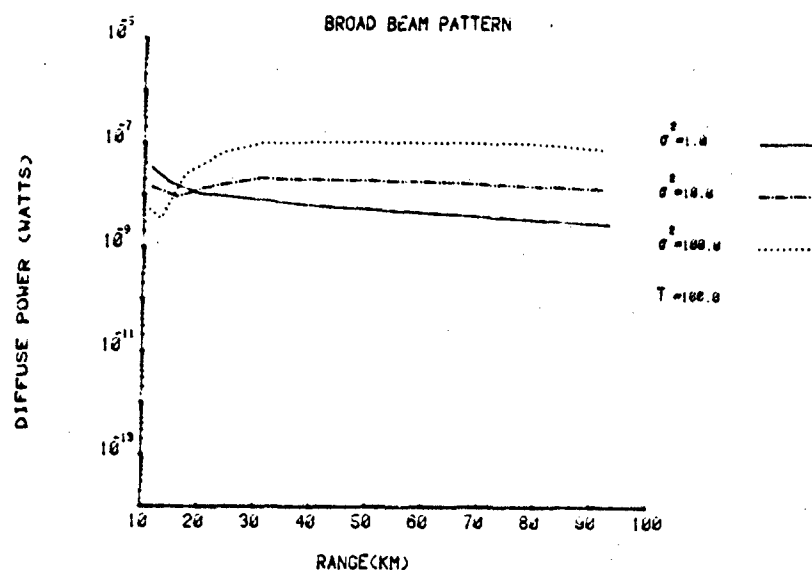
Figure 6. Diffuse Power Behavior for a Centrally-uniform Power Pattern; Standard Glistening Surface, $T = 100$ m, $\sigma^2 = 1, 10, 100$ m^2

30

COMPARISON OF DIFFUSE POWER DATA AND RESULTS FROM THEORETICAL MODELS
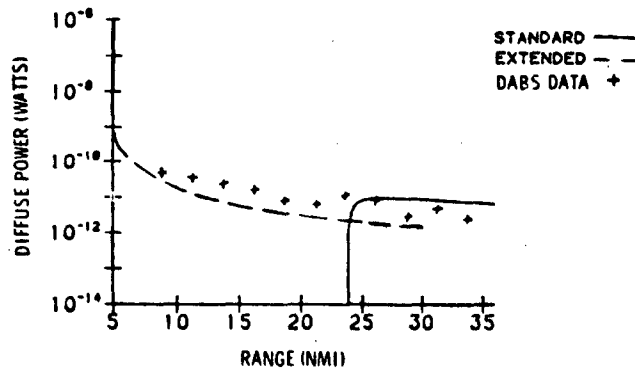
Figure 7. Comparison Between Standard Glistening Surface,
Full Integration, and DABS Data: Diffuse Scattered Power
vs Range

The results of the terrain data base analysis are recorded on a computer tape
for use with the computer program for the electromagnetic analysis (see Appen-
dix A). The dashed line in Figure 7 shows the diffuse power predicted by the com-
puter model when the extended length and width glistening surface is used. The
solid line shows the diffuse power predicted by the computer model when the
Beckmann and Spizzichino[1] definition of glistening surface is used. It may be
noted from this figure that the extended glistening surface model shows remark-
able agreement with experimental data for all ranges between transmitter and
receiver. On the other hand, the standard glistening surface model shows poor
agreement with the experimental data particularly at short ranges.

4. MOISTURE EFFECTS

In this section we are concerned with the behavior of the scattering surface
when there is a range of moisture levels present. The moisture is represented
by assigning different dielectric constants to the surface. This effect is examined
for various roughness levels. Both definitions of the glistening surface are used
and their results compared (Appendix A and Appendix C).

In previous studies[7,19] we have used the appropriate dielectric constants for
the terrain as described by the geologic coding of the DABS site data base. When
we turned to the question of glistening surface limitations,[8] we used both the DABS
values and a number of cases where the entire surface was assumed to be of uni-
form roughness and to be cultivated terrain with complex dielectric constant,

31

$\epsilon_r = 80 + j\ 9.0$. In this present instance, we use three soil descriptors reflecting different moisture levels and consider how the relative roughness affects the scattering. For dry desert-type sandy soil we used $\epsilon_r(1) = 2 + j\ 1.62$, for ordinary dry ground $\epsilon_r(2) = 4 + j\ 0.006$, and for moist soil $\epsilon_r(3) = 30 + j\ 0.6$.[3]

Figure 8 shows several aspects of the effect of moisture content on the scattering. The two upper illustrations and the lower left-hand side illustration show the progression in behavior of the range-dependent diffuse scattered power when $\sigma^2 = 10\ m^2$ and T is varied from $1.0\ m \leq T \leq 500\ m$. The three cases are for the extended definition of glistening surface. The final illustration of the figure shows the solution for the standard definition of the glistening surface with T = 500 m.

If we examine the three dielectric constants used here we see that, although the relative change in the imaginary components is greater than that for the real parts, the absolute levels are smaller in magnitude than the real contributions and thus the differences in the diffuse power follow the real part of the dielectric constant for the particular set of soil types investigated in this study.
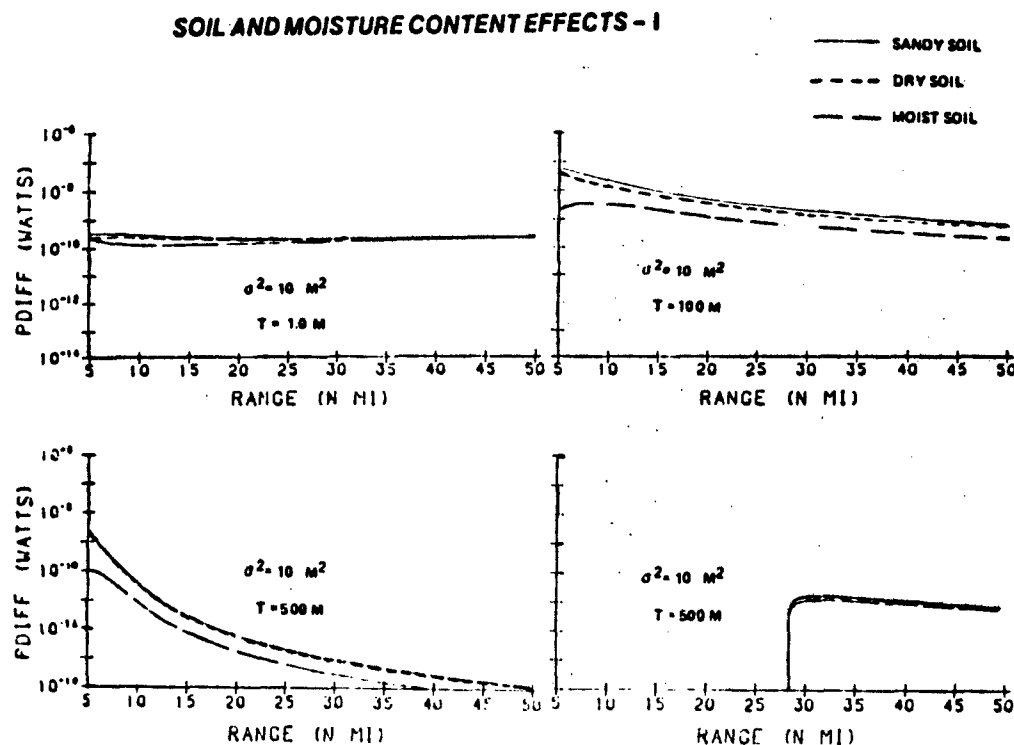

Figure 8. Soil and Moisture Effects on Diffuse Power: Full Integration - $\sigma^2 = 10\ m^2$, T = 1, 100, 500 m; Standard Surface - $\sigma^2 = 10\ m^2$, T = 500 m

The next factor to note is that, for the extended surface case, as the value of T increases from T = 1 m to T = 500 m for the extended surface case, several differences in behavior can be seen. First, the respective sets of curves show increased rates of dropoff with increasing range. Next, the magnitudes pass through a peak at the intermediate σ/T ratio. Finally, the effect of moisture content on the diffuse power increases as T increases.

The standard glistening-surface results for T = 500 m differ from equivalent results with the extended glistening surface definition as is expected. For the standard case there is the typical cutoff at 28 nmi and the overprediction of the diffuse power at long ranges.[8] Here, the interest is in the effect of moisture level. For the assumptions of the standard glistening-surface model, the three moisture curves reveal only slight variations in diffuse power. In contrast, for the extended surface model there is considerable moisture dependence for the scattered power (differences of as much as an order of magnitude). This is a rather significant finding. One would ordinarily expect that the relative spread in the scattered power would be equivalent in the two models. Some analysis of the situation will be useful in explaining this behavior.

The analysis involves how the moisture levels enter the calculation and how the two versions use the moisture dependent terms to arrive at the diffuse power levels scattered by the surface. These topics are addressed in the discussions of the differences between the two scattering models contained in Appendix C. There it is shown that the dielectric constant is introduced as a term in the Fresnel reflection coefficients. Then, consideration of the two distinct versions of the scattering matrix elements indicates how the difference in behavior occurs. In the standard model the scattering elements each contain only one of the Fresnel coefficients, while in the extended version each element depends on both Fresnel coefficients. In addition, for the standard solution the final result for the diffuse power is based on the centerline σ° variation multiplied by the glistening surface width at each point. For the extended solution the result includes the scattering element contribution at each azimuthal position. This introduces a whole range of weighted, moisture-dependent terms related to the angular variation.

One specific aspect of the particular antenna system used in the study might suggest that these results are only valid in this instance. That aspect is the receiving antenna azimuthal power pattern (see Figure 2). The pattern contains a centerline null that removes the centerline σ° contribution from the total diffuse power calculated using the extended surface model. The question is whether it is the aspect that allows the azimuthal contributions to dominate the diffuse power result and, consequently, whether there would be moisture-related differences between the two models if alternative azimuthal power patterns were considered.

To answer that quest on the original power pattern was replaced by one having its peak at the centerline; it then remains at that level over a considerable fraction of the entire pattern. When the diffuse power was calculated for the new power pattern using both models, differences in the moisture behavior between the two models still occurred. Figure 9 shows this result for the case where $\sigma^2 = 10 \text{ m}^2$ and T = 100 m. For the two antenna azimuthal power patterns, diffuse power levels are presented for both the standard surface and the extended one. Close examination of these results indicates that the second power pattern results in less of a difference in moisture effects than the original. Nevertheless, even with centerline contributions, the extended glistening-surface solution has a greater variation with moisture level than does the standard surface solution.
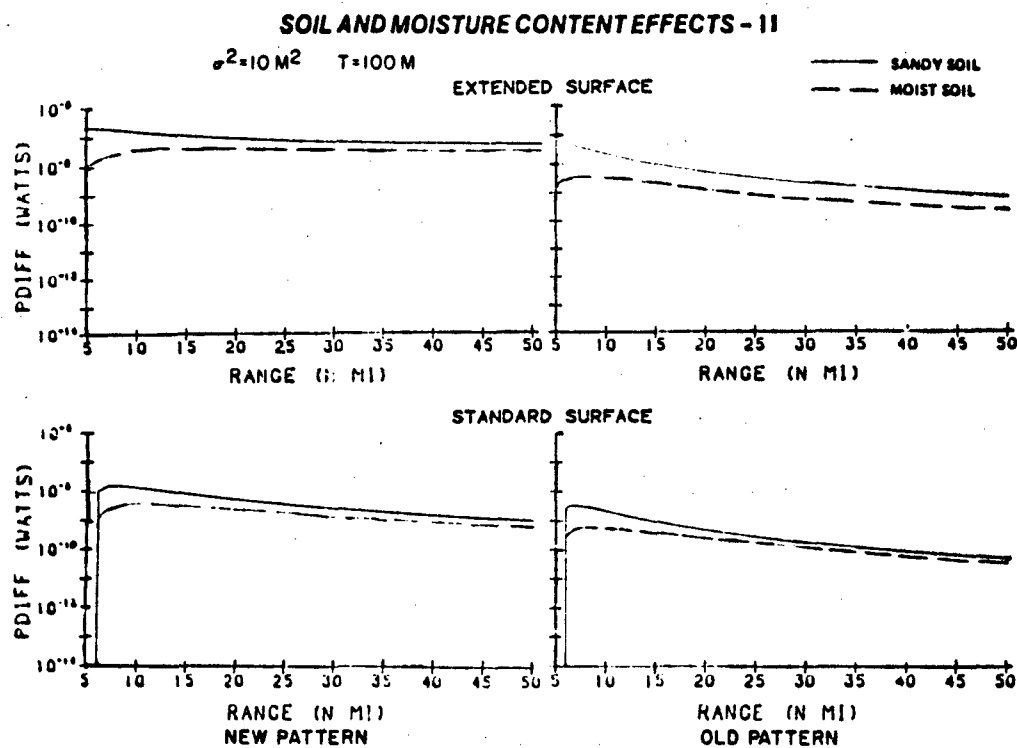
Figure 9. Soil and Moisture Effects on Diffuse Power, $\sigma^2 = 10 \text{ m}^2$, T = 100 m: Both Antenna Patters, Standard Surface, and Full Integration Models

The final area of the moisture analysis is a summarization of the effects for
the two glistening-surface definitions as a function of roughness. This compilation
of results is presented in Figure 10. The extended surface results for the two
moisture extremes are shown on the left of this figure, while the corresponding
standard glistening-surface results are shown on the right. Each graph contains
separate curves of the diffuse power behavior at three antenna separations as a
function of a roughness factor, σ/T. This represents a highly-compressed de-
scription of the results, and the information requires detailed discussion.

SOIL AND MOISTURE CONTENT EFFECTS III

EXTENDED SURFACE   STANDARD SURFACE
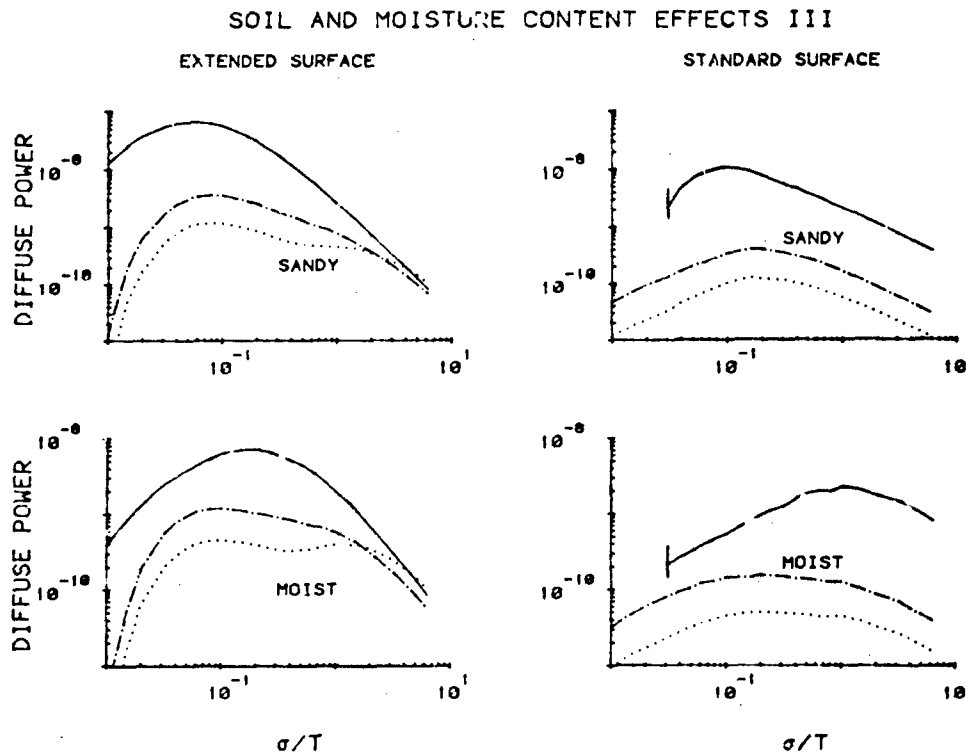
Figure 10. Soil and Moisture Effects on Diffuse Power as a Function of σ/T
Ratio at Three Antenna Separations: Standard Surface and Full Integration
Models - (5 nmi ———; 30 nmi —.—; 50 nmi ....)

If we first examine the two surfaces separately, we see that the trends for the
σ/T dependence are relatively similar for the three separations. The behavior is
not the same, though, if we compare the results for the two definitions. The ex-
tended surface results in larger diffuse power levels than those from the corre-
sponding standard surface. In addition, the extended surface result peaks at lower

35

σ/T values than does the standard case, and we can see differences in behavior at large σ/T values. The two definitions produce significantly different patterns in this range. For the extended case, the curves at the three antenna separations all tend to converge for large σ/T. This holds for both moisture levels. On the other hand, for the standard case the two sets of moisture levels result in parallel behavior for large σ/T values, although the moist surface behavior is more complex. For the standard case an additional anomaly is apparent at the opposite end of the σ/T range. There, the results for the 5-nmi case are no longer simila. to the 30- and 50-nmi cases. This is a result of the vanishing of the glistening surface that tends to occur at larger ranges as the σ/T ratio decreases. This subject is discussed in detail in our previous report,[8] but the trend can be seen here by consideration of the standard glistening surface cases in Figure 3. This figure shows the change in glistening surface cutoff for $\sigma^2 = 10\ m^2$ as T changes from T = 100 m to T = 500 m.

There is no simple statement that generalizes the wide range of moisture-related effects and their dependence on the definition of glistening surface and scattering model. It should just be noted that there is a strong roughness effect and that the two models can yield quite different results for some σ/T ranges.

There are several implications for radar applications in these results. The first point is that knowledge of the moisture content is not sufficient for absolute prediction of the results of system performance. For different roughness levels the effect of moisture can be quite different. The second point is that moisture effects based on standard calculations may be at variance with the predictions obtained for the effects of moisture on diffuse scattering when the extended surface is used in the analysis.

5. CONCLUSIONS

In this report we have examined our rough surface scattering theory in terms of its underlying principles and assumptions and established that the assumed level of surface roughness has a highly significant effect on the overall solution. The results of the analysis reflect a wide range of topics. In this section we will summarize these results and their implications.

The first area is the discussion of the various theoretical formulations and the conditions for their validity. The two main theories for scattering are the perturbation theory, which requires the surface irregularities to be small compared to a wavelength with the surface slopes less than unity, and the physical optics approximation where the radii of curvature of the irregularities are large compared to a wavelength and the surface slopes less than unity. Additional

factors that can effect the results are multiple scales of roughness and differences in the statistical characterization of the scattering surface. Among the more significant statistical aspects is the property that for some distributions, uncorrelated surface heights are independent while for other cases this condition is not satisfied. In the present discussions conditions for physical optics are always assumed to apply. Then the surface cross section $\sigma^\circ = [\beta_{ij}]^2 J$ depends on the scattering matrix and the statistical form J. A major concern of this study is to examine the agreement and limitations for the alternative J-representations as a function of Rayleigh parameter, Σ.

For Gaussian surfaces when $\Sigma \gg 1$, the summation result is poor while the asymptotic and integral results agree. In this case the agreement is independent of azimuthal scattering angle. These solutions diverge as Σ decreases, and the summed result agrees with the integral. In the ranges where $\Sigma \leq 1$, the summation result has become the only usable representation because the behavior of the kernel in the integral formulation makes accurate numerical evaluation of the integral intractable.

For exponential surfaces the results are slightly different. In that instance, the integral form is accurate over the entire range of Σ values. The asymptotic solution agrees with the integral one for large Σ, with the summation being completely at variance. In contrast, the $\Sigma \leq 1$ the asymptotic solution does not agree with the integral result while the power series expansion solution does. Again, there is no apparent trend related to the magnitude of the azimuthal scattering angle.

The next area of interest is that of the concept of glistening surface. The extent of the surface and the inclusion of the related scattered power in the theories used in our analyses has progressed through several stages. The differences in results are clearly roughness dependent.

The standard glistening surface as described in Beckmann and Spizzichino[1] generates reasonable results for a wide range of conditions, particularly for large σ/T ratios. We found that for small σ/T ratios, though, the length of the glistening surface either vanished or omitted significant portions of the surface between the two antennas. Extension of the glistening surface to include scattering contributions from the entire surface between the antennas has shown that the power from these excluded areas could be quite significant for some conditions. This represented the first modification of the formalism.

The original Beckmann and Spizzichino solution assumes that the azimuthal variation of the cross section is negligible and determines the result by considering the product of the centerline ($\phi_s = 0$, boresight direction) σ° values at any point along the length of the glistening surface and its associated width at that point. In the initial modification, this assumption was maintained. The newest

modification relaxes this constraint. As in the previous case the integration is along the entire separation between antennas. Here the concept of specific surface width is removed, and the integration is carried out over the azimuthal extent of the power pattern. Also, an associated azimuthally varying value for the cross section of the surface is included in the theory. It was found that for small σ/T ratios the standard solution approximations result in over-prediction at large antenna distances and underprediction at short ranges. For larger σ/T values the results tended to agree.

For the above results, the azimuthal variation in σ° is modified by the corresponding azimuthal power pattern of the receiver. This suggested considering the effect of a drastically different azimuthal power pattern. Specifically, instead of a monopulse pattern, a pattern was chosen that has an essentially constant value over the typical azimuthal extent of significant cross section values. The results followed the same trends as before except that the full integration is always greater than the standard glistening surface results. In the case of large σ/T ratio, the centerline null in the original pattern resulted in relative agreement for the two models. (The centerline null in the pattern balances the omitted surface area.) Here, the peak centerline value adds to the difference, and the full integration results remain higher. The final point with respect to the different glistening surface results is that the full integration case gives excellent agreement with the DABS data while the standard surface results show areas of poor agreement particularly at short ranges.

Once we established the effects of roughness on the agreement between theories, the final topic of the present study was introduced. This is the effect of roughness on the results when the moisture content of the surface is varied.

A number of results were found. For the azimuthal difference power pattern, a decrease in the value of σ/T resulted in increased variation between the successive moisture level values for scattered power as a function of antenna separation. For small σ/T values the difference between the moisture level results of the full glistening surface and the standard surface is considerable. The behavior of the diffuse power as a function of moisture content and surface roughness at given antenna separations is quite dissimilar for the two definitions of glistening surface. This is particularly true for extremes of large and small σ/T.

The centerline power pattern null tends to emphasize differences between results from the two models, but the introduction of the alternative azimuthal pattern still resulted in differences in the effect of moisture.

As a result of these studies of roughness dependent effects on scattering it is clear that use of simplified models for the scattering surface can lead to considerable errors in the prediction of the scattered power, most notably for small σ/T roughness parameter conditions. In addition, the effect of moisture is quite

different depending on the glistening surface model particularly at the extremes of either large or small σ/T ratio.

Predictive models of radar performance that do not properly account for diffuse scattered power can lead to design criteria that may either be more expensive then necessary or result in poor operational performance. The moisture dependence on roughness also suggests that there can be inadequate estimation of performance variability, unless those effects are properly taken into account.

References

1. Beckmann, P., and Spizzichino, A. (1963) The Scattering of Electromagnetic Waves From Rough Surfaces, Macmillan Co., New York.

2. Ruck, G.T., Barrick, D.E., Stuart, W.D., and Krichbaum, C.K. (1970) Radar Cross Section Handbook, Vol. 2. Plenum Press, New York.

3. Long, N.W. (1975) Radar Reflectivity of Land and Sea, Lexington Books, Lexington, Mass.

4. Brown, G.S. (19--) A stochastic Fourier transform approach to scattering from perfectly conducting randomly rough surfaces, IEEE Trans. Antennas Propag. (to be published).

5. Peake, W.H. (1959) The Interaction of Electromagnetic Waves With Some Natural Surfaces, Antenna Laboratory, Ohio State University Report-898-2.

6. Papa, R.J., and Lennon, J.F. (1980) Electromagnetic scattering from rough surfaces based on statistical characterization of the terrain, International Radio Science Symposium, (URSI), June 1980, Quebec, Canada.

7. Papa, R.J., Lennon, J.F., and Taylor, R.L. (1980) Electromagnetic Wave Scattering From Rough Terrain, RADC-TR-80-300, AD-A-09839.

8. Papa, R.J., Lennon, J.F., and Taylor, R.L. (1982) The Need For An Expanded Definition of Glistening Surface, RADC-TR-82-271.

9. Rice, S.D. (1951) Reflection of electromagnetic waves by slightly rough surfaces, The Theory of Electromagnetic Waves, M. Kline, Ed., Wiley, New York.

10. Wright, J.W. (1966) Backscattering from capillary waves with application to sea clutter, IEEE Trans. Antennas Propag. AP-14:749.

11. Fuks, I M. (1966) Contribution to the theory of radio wave scattering on the perturbed sea surface, Izvestia Vyshikh Uchebnykh Zavedenii Radiofizika 5:876.

12. Brown, G.S. (1973) Backscattering from a Gaussian distributed perfectly conducting rough surface, IEEE Trans. Antennas Propag. AP-26:472.

13. Burrows, M. L. (1967) A reformulated boundary perturbation theory in electromagnetism and its application to a sphere, *Can. J. Phys.* 45:1729.

14. Bahar, E. (1981) Scattering cross sections for random rough surfaces: Full wave analysis, *Radio Sci.* 16:331-341.

15. Barrick, D. E. (1965) *A More Exact Theory of Backscattering From Statistically Rough Surfaces*, Ohio State University Research Foundation, Report 1388-18.

16. Ott, R. H. (1967) *A Theoretical Model for Scattering From Rough Surfaces With Applications to the Moon and Sea*, Ohio State University Research Foundation, Report-1388-1.

17. Beckmann, P. (1973) Scattering by non-Gaussian surfaces, *IEEE Trans. Antennas Propag.* AP-21:169.

18. Lennon, J. F., and Papa, R. J. (1980) *Statistical Characterization of Rough Terrain*, RADC-TR-80-9, AD A087746.

19. Papa, R. J., Lennon, J. F., and Taylor, R. L. (1980) *Prediction of Electromagnetic Scattering for Rough Terrain Using Statistical Parameters Derived From Digitized Topographic Maps*, RADC-TR-80-289, AD A094104.

20. McGarty, T. P. (1975) *The Statistical Characteristics of Diffuse Multipath and Its Effect on Antenna Performance*, ESD-TR-75-145, AD A009869.

21. Brown, G. S. (1982) Scattering from a class of randomly rough surfaces, *Radio Sci.* (To be published).

Appendix A

Description of Rough Surface Scattering Analysis

In this appendix we describe the details of the surface scattering formalism in terms that are common to the two basic versions of the program used to obtain the results found in this report. Additional discussions of distinctions between the two models will be discussed in Appendix C.

The common elements involve the calculation of the specular and diffuse scattering from rough terrain, which incorporates statistical parameter estimation applied to digitized terrain data bases. The terrain is divided into homogeneous, isotropic, rectangular cells, that are each characterized by a mean height, variance, degree of correlation, statistical height distribution, and an appropriate dielectric constant. The model includes spatial inhomogeneities from cell to cell, multiple specular reflection points, and global and local shadowing with explicit shadowing functions for Gaussian and exponentially-distributed surface heights. The antenna power patterns of both the transmitter and monopulse receiver are included in the model, and signal processing losses can be considered.

The programs normally use system parameters associated with the L-band Discrete Address Beacon System (DABS) to allow comparisons with experiment. These are defined in Table A1 and Figure 8. External inputs include the complex dielectric constant for each surface area, the coordinates of the monopulse receiver, the velocity and initial and final positions of the aircraft containing the transmitter, and a parameter to control the effects of shadowing.

43

Table A1. Experimental Conditions for Discrete Address Beacon System Tests

Front-end receiver noise figure	3 dB
Gain of monopulse receiver (sum pattern) antenna	22.5 dB
Gain of transmitter antenna	4 dB
Height of receiver antenna	101 m
Height of transmitter antenna	1220 m
Signal polarization	vertical
Peak transmitter power	350 W
Pulse length	20 μsec
Azimuthal beamwidth (receiver)	3°
Wavelength	0.275 m
Transmission line loss factor	3 dB
System processing loss	2 dB
Normalized pattern slope	1.5

The description of the models may be divided into two major topics. These are the techniques required to assign appropriate statistical properties to the terrain and the specifics of the electromagnetic formulation. Each of these aspects requires some discussion.

There are several surface feature contributions in the models. Analyses of the scattering from rough surfaces consider the surface heights in the region as pairs of scattering elements and in most cases, including this study, assume that the height distribution can be described by either a bivariate Gaussian or exponential probability density. These two bivariate densities have the forms:

(Gaussian)

$$p(Z_1, Z_2) = \left(\frac{1}{2\pi\sigma^2\sqrt{1-C^2}}\right) \exp\left[-\left(\frac{(Z_1-\mu_1)^2 - 2C(Z_1-\mu_1)(Z_2-\mu_2) + (Z_2-\mu_2)^2}{2\sigma^2(1-C^2)}\right)\right]$$

(A1)

44

(Exponential)

$$p(Z_1, Z_2) = \left(\frac{3}{2\pi\sigma^2\sqrt{1-C^2}}\right) \exp\left[-\left(\frac{(Z_1-\mu_1)^2 - 2C(Z_1-\mu_1)(Z_2-\mu_2) + (Z_2-\mu_2)^2}{(1/3)\sigma^2(1-C^2)}\right)^{\frac{1}{2}}\right].$$

(A2)

Both forms have the same set of defining parameters, the mean height μ, the variance σ^2, and the correlation function C.

In the present analysis, either the form of the density function and its associated parameters are assigned as initial conditions of the problem or, if a specific site is being analyzed, the probability density and the values for its parameters are determined by statistical techniques. The procedures for describing a site have been discussed in some detail in earlier work.[A1, A2] A brief outline will be included here. The theoretical formulations will be described, followed by a discussion of their application to actual terrain.

The starting point of the analysis is to determine appropriate estimators for the parameters of a Gaussian or exponential density. We consider that we have sample height values from the population of the region. The sample mean is then used as the estimator for the population mean height and the sample variance is used as the estimator for the population variance. A more complicated development is required to establish values for a normalized covariance estimator.[A3] This is then used to obtain the correlation length, T.

The next step is to decide which density is more appropriate. Different decision models have been developed.[A3] One such approach is the following. If the heights in a region are described by a particular bivariate form when considered in pairs, then the population as a whole should be described by a higher-order multivariate density that has the required bivariate marginal density. A hypothesis testing procedure is then applied to the two alternative multivariate densities that describe the entire collection of height values in the region simultaneously. This

A1. Papa, R.J., and Lennon, J.F. (1980) Electromagnetic scattering from rough surfaces based on statistical characterization of the terrain, International Radio Science Symposium, (URSI), June 1980, Quebec, Canada.

A2. Papa, R.J., Lennon, J.F., and Taylor, R.L. (1980) Prediction of Electromagnetic Scattering For Rough Terrain Using Statistical Parameters Derived From Digitized Topographic Maps, RADC-TR-80-289, AD A094104.

A3. Papa, R.J., Lennon, J.F., and Taylor, R.L. (1980) Electromagnetic Wave Scattering From Rough Terrain, RADC-TR-80-300, AD A09839.

simple alternative hypothesis test is equivalent to a minimum-error probability criterion where it is equally likely that either density is the appropriate one.

For the comparison of the scattering theory with the experiment, these techniques had to be applied to the terrain at the eastern Massachusetts site. A data base of topographic elevations for this area is available at the Electromagnetic Compatibility Analysis Center (ECAC) in Annapolis, Md. This was prepared from digitized terrain maps supplied by the Defense Mapping Agency (DMA). The area of interest is divided into rectangular cells, each with sides of about 2 km. Each cell is further subdivided into a 10 by 10 grid of points. The statistical analysis is then applied to the individual cells.

The statistical data for each cell has been recorded on a computer tape for use with the program for the electromagnetic analysis. Each cell is represented by seven descriptors. The first two entries are the (x, y) coordinates for the center of the cell. Next is the geological code (dielectric constant) for the cell. (The predominant feature is woods; there are a number of cells containing clusters of lakes and ponds and a few town sites with associated cleared areas.) This is followed by the mean and variance of the heights in the cell and the estimated correlation length, T (the units of length are in meters). The final quantity is the result of the hypothesis test.

The trajectory of the beacon aircraft is incorporated into the computer program and at each range point for which a calculation is to be made, the required cells and their descriptors are then identified. These results or, in the general case, the equivalent set of input parameters are then used in the electromagnetic analysis.

The calculation of the electromagnetic fields has two distinct elements. First, the total coherent electric field E_{COH} at the receiver is calculated by using the sum pattern of the receiver antenna in the following expression:

$$E_{COH} = E_T \left[1 + \sum_j G_j(\theta_m) \widetilde{R}_j \Gamma_{F_j} e^{ik\Delta R} \right] , \tag{A3}$$

where

E_T = direct path electric field at the receiver,

$G_j(\theta_m)$ = gain of receiver in direction of multipath ray, where θ_m is the angle between the direct ray and multipath ray,

$\widetilde{R}_j$ = attenuation factor affecting coherent reflected wave due to surface roughness,

Γ_{F_j} = complex Fresnel plane wave reflection coefficients,

46

$k \qquad = 2\pi/\lambda$, and

$\Delta R \qquad$ = difference in path length between direct ray and reflected ray.

The summation over j represents all possible specular reflections (there may be more than one, due to unevenness in terrain). Here, coherence means there is a known phase relationship between the em field leaving the transmitter and that reaching the receiver.

The next aspect is that of the diffuse power. The diffuse power in the monopulse difference channel is calculated from the expression

$$P_{DIFF} = \left(\frac{P_T X_{LOSS} \lambda^2}{(4\pi)^3} \right) \iint \left(\frac{G_{TR}^{AZ}(\phi_2) G_R^{AZ}(\phi_1)}{R_1^2 R_2^2} \right) \cdot$$

$$\left(G_{TR}^{EL}(\theta_1) G_R^{EL}(\theta_2) \ \sigma^\circ(\theta_1, \theta_2, \phi_1) \right) \ dS \quad , \ (A4)$$

where

X_{LOSS} = system processing losses

$P_T \qquad$ = transmitted power,

$\lambda \qquad$ = wavelength,

$G_{TR}^{AZ} \qquad$ = gain (power) of transmitter in azimuth (isotropic pattern),

$G_R^{AZ} \qquad$ = gain of receiver in azimuth (difference pattern, Figure 8),

$G_{TR}^{EL} \qquad$ = gain of transmitter in elevation (isotropic pattern),

$G_R^{EL} \qquad$ = gain of receiver in elevation (Figure 8),

$\theta_1 \qquad$ = elevation angle between boresight and point on glistening surface for transmitter,

$\theta_2 \qquad$ = elevation angle between boresight and point on glistening surface for receiver,

$R_1 \qquad$ = range between transmitter and point on glistening surface,

$R_2 \qquad$ = range between receiver and point on glistening surface,

$dS \qquad$ = element of area of glistening surface which is illuminated by beacon,

$\phi_1 \qquad$ = azimuthal angle between boresight and point on glistening surface for receiver, and

47

ϕ_2 = azimuthal angle between boresight and point on glistening surface for transmitter.

The diffuse power integral contains an expression for the normalized average bistatic rough-surface cross-section, $\sigma°$, which comes from Ruck et al.[A4] The expressions derived by Ruck are quite general and highly complicated. The different forms of $\sigma°$ used in the models will be discussed in Appendix C. Here we will simply comment that

$$\sigma° = |\beta_{pq}|^2 \, J \, S \quad ,$$

where β_{pq} represents the scattering matrix and S introduces the local shadowing contribution. The term J is related to the surface height distributions and the surface slopes. For a Gaussian surface

$$J = \left(\frac{T^2}{\sigma^2 \xi_z^2} \right) \exp \left[- \left(\frac{T^2}{4\sigma^2} \right) \left(\frac{\xi_x^2 + \xi_y^2}{\xi_z^2} \right) \right]$$

and for an exponential surface height probability density

$$J = \left(\frac{3T^2}{\sigma^2 \xi_z^2} \right) \exp \left[- \left(\frac{\sqrt{6} \, T}{2\sigma} \right) \left(\frac{\xi_x^2 + \xi_y^2}{\xi_z^2} \right)^{1/2} \right] \quad ,$$

where

$\xi_x = \sin \theta_1 - \sin \theta_s \cos \phi_s$,

$\xi_y = \sin \phi_s \sin \theta_s$,

$\xi_z = -\cos \theta_i - \cos \theta_s$,

ϕ_s = azimuthal scattering angle,

θ_i = angle of incidence (with respect to surface normal), and

θ_s = angle of scattering (with respect to surface normal).

The final aspects of the model is the azimuthal angle error. To calculate this, we assume that the spectral width of the diffuse multipath is narrow compared to the bandwidth of the receiver/processor, and that both noise power and diffuse multipath power are Rayleigh distributed. For the conditions of the DABS system,

A4. Ruck, G. T., Barrick, D. E., Stuart, W. D., and Krichbaum, C. K. (1970) Radar Cross Section Handbook, Vol. 2, Plenum Press, New York.

the decorrelation time of the diffuse multipath power is of the order of 10^{-2} sec, and the interpulse period is of the order of 10^{-6} sec. Also, for the DABS experiment test site, the spectral width of the diffuse multipath power is of the order of 100 Hz, and the bandwidth of the receiver processor is about 5×10^4 Hz. This shows why even narrowband Doppler filtering cannot reduce the diffuse multipath power in the radar resolution cell containing the target. Under these conditions, the total amount of noiselike interference N_I in the radar resolution cell containing the signal is given by

$$N_I = P_{DIFF} + N_o \quad , \tag{A5}$$

where

N_o = noise power from environment plus receiver.

The error, σ_θ, in azimuthal angle pointing accuracy is given by the expression of Barton and Ward[A5]:

$$\sigma_\theta = \left(\frac{\theta_B}{k_m \sqrt{2STIR}} \right) \quad . \tag{A6}$$

where

θ_B = azimuthal beamwidth,

STIR = P_{COH}/N_I = signal to interference ratio in the difference channel,

P_{COH} = coherent power in sum channel, and

k_m = normalized pattern slope.

A5. Barton, D.K., and Ward, H.R. (1969) Handbook of Radar Measurement, Prentice-Hall Inc., Englewood Cliffs, New Jersey.

References

A1. Papa, R.J., and Lennon, J.F. (1980) Electromagnetic scattering from rough surfaces based on statistical characterization of the terrain, International Radio Science Symposium, (URSI), June 1980, Quebec, Canada.

A2. Papa, R.J., Lennon, J.F., and Taylor, R.L. (1980) Prediction of Electromagnetic Scattering For Rough Terrain Using Statistical Parameters Derived From Digitized Topographic Maps, RADC-TR-80-289, AD A094104.

A3. Papa, R.J., Lennon, J.F., and Taylor, R.L. (1980) Electromagnetic Wave Scattering From Rough Terrain, RADC-TR-80-300, AD A09839.

A4. Ruck, G.T., Barrick, D.E., Stuart, W.D., and Krichbaum, C.K. (1970) Radar Cross Section Handbook, Vol. 2, Plenum Press, New York.

A5. Barton, D.K., and Ward, H.R. (1969) Handbook of Radar Measurement, Prentice-Hall Inc., Englewood Cliffs, New Jersey.

51

Appendix B

Derivation of Expressions for Normalized Cross Sections
of Rough Surfaces

In this appendix, the expressions for the normalized cross section σ° of a rough surface are derived for bivariate Gaussian-distributed surface heights and also for bivariate exponentially-distributed surface heights. The approximation of physical optics is assumed to apply. Under the assumptions of physical optics the expression for σ° may be written

$$\sigma^\circ = \left| \beta_{pq} \right|^2 J S \quad .$$

The scattering matrix, $\left| \beta_{pq} \right|$ and the shadowing function, S are discussed in Appendix A and Appendix C. Here the discussion will be limited to the final term in the expression for σ°, the J factor. In Appendix A we discuss, for both distributions, the particular form for J that applies for large values of the Rayleigh roughness parameter $[\Sigma = (2\pi\sigma/\lambda)(\cos\theta_i + \cos\theta_s)]$. Here, the discussion is broadened to other regimes and the form for the J term is derived for large Rayleigh parameter, $\Sigma \gg 1$; intermediate Rayleigh parameter, $\Sigma \approx 1$; and small Rayleigh parameter, $\Sigma < 1$. It should be mentioned at this point that when the Rayleigh parameter is large, a formulation of the rough surface scattering problem, which is more complete than the physical optics approach, shows that

PREVIOUS PAGE
IS BLANK

multiple scattering becomes important. In particular, DeSanto and Shisha[B1] showed, by numerically solving an integral equation, that for a Gaussian distributed surface with large surface roughness (large Rayleigh parameter) and small correlation length, single scattering grossly underestimated the strength of the average scattered field. Recently, for a rough surface having a correlation length much smaller than the em wavelength, Brown[B2] has shown that an analysis may be used based on a substitute surface which gives rise to the same average scattered field as the true surface. It is demonstrated that the average scattered field depends upon the number of interacting areas and the surface roughness. There is a specific number of interacting areas that dominate the average scattered field for a given range of Rayleigh parameter Σ. The number of interacting areas increases as the Rayleigh parameter increases.

In the present report, no multiple scattering is considered and the approximations of physical optics are used to derive the expressions for σ° when the surface heights have different distribution functions. Different expressions are obtained for σ° as a function of the value of the Rayleigh parameter. (In Section 2 of this report, each of the expressions for σ^2 is evaluated over a wide range of the Rayleigh parameter to assess the regions of validity for the different relations and the extent of the disagreement among the σ^2 values.) The differences in σ^2 are considered to be related to the differences in the J-values for the three Σ-regimes. The generalized integral formulation for J is given by

$$J = \left(\frac{4\pi}{\lambda^2}\right)\left(\frac{1}{A}\right) \int_{-X}^{X} dx_1 \int_{-X}^{X} dx_2 \int_{-Y}^{Y} dy_1 \int_{-Y}^{Y} dy_2 \left[\exp\left\{i\left[v_x(x_2 - x_1) + v_y(y_2 - y_1)\right]\right\}\right] \cdot$$

$$\left[\chi_2 - \chi \chi^*\right] \quad , \qquad (B1)$$

where

$$A = 4XY$$

$$v_x = \left(\frac{2\pi}{\lambda}\right)(\sin\theta_i - \sin\theta_s \cos\phi_s)$$

B1. DeSanto, J.A., and Shisha, O. (1974) Numerical solution of a singular integral equation in random rough surface scattering theory. J. Comp. Phys. 15(No. 2):286.

B2. Brown, G.S. (1982) New results on coherent scattering from randomly rough conducting surfaces, IEEE Trans. Antennas Propag. (to be published).

$$v_y = \frac{-2\pi}{\lambda}(\sin\theta_s \sin\phi_s) \quad ,$$

θ_i = angle of incidence with respect to surface normal ,

θ_s = angle of scattering with respect to surface normal ,

ϕ_s = azimuthal scattering angle ,

χ = marginal univariate characteristic function ,

χ_2 = bivariate characteristic function ,

λ = em wavelength ,

2X = length of rough surface ,   and

2Y = width of rough surface .

This expression for J involves no assumptions about the surface height distribution or the size of the Rayleigh parameter (the only restrictions are that the radius of curvature of the irregularities on the surface be large compared to a wavelength and that the surface slopes are small, $\sigma/T \ll 1$).

The next step is to evaluate the integral for specific cases. We first note that the bivariate characteristic function (the Fourier transform of the bivariate surface-face height distribution function) is a function of the correlation coefficient $c(\tau)$ where τ is the separation of two points on the surface

$$\tau = \sqrt{(x_1 - x_2)^2 + (y_1 - y_2)^2} \quad .$$

The following results are for the Gaussian form, $c(\tau) = \exp[-\tau^2/T^2]$. The correlation coefficient has the following properties: $c(0) = 1$, $c(\tau \to \infty) \to 0$, and $0 \le |c| \le 1$. This behavior will be used in the specific deviations.

The first case that we will consider is the form for the Gaussian surface-height distribution. The three different ranges of Σ are covered in succession. A discussion of this case is presented in the book by Beckmann and Spizzichino.[B3] The present development is given to clarify the comparisons in Section 2 and to show the similarities and differences between these results and those for the exponential distribution.

For the bivariate Gaussian surface-height distribution function as given in Appendix A, the corresponding characteristic function is given by

$$\chi_2 = \exp[-\Sigma^2(1 - c(\tau)]$$

B3. Beckmann, P., and Spizzichino, A. (1963) The Scattering of Electromagnetic Waves From Rough Surfaces, Macmillan Co., New York.

and the corresponding univariate characteristic function is given by

$$\chi = \exp[-\Sigma^2/2] \quad .$$

For the Gaussian distributed surface heights

$$\chi_2(\tau \to \infty) \to \chi \chi^*$$

that is, decorrelation leads to statistical independence. Because of this fact the previous integral for J may be readily reduced to the following form:

$$J = \frac{8\pi^2}{\lambda^2} \int_0^\infty J_0(v_{xy}\tau)[\chi_2 - \chi\chi^*]\,\tau\,d\tau \quad , \tag{B2}$$

where $v_{xy} = v_x^2 + v_y^2$.

If the Rayleigh parameter $\Sigma \gg 1$, a steepest descent evaluation of the integral shows that most of the contribution comes from $\tau \approx 0$. Then
$c(\tau) = \exp[-\tau^2/T^2] \approx [1 - \tau^2/T^2] \Rightarrow \chi_2 \approx \exp(-\Sigma^2\tau^2/T^2)$ and $\chi\chi^* \approx 0$ so that

$$J = \frac{8\pi^2}{\lambda^2} \int_0^\infty J_0(v_{xy}\tau) \exp[-\Sigma^2\tau^2/T^2]\,\tau\,d\tau$$

and after integration,

$$J = \left(\frac{4\pi^2 T^2}{\lambda^2 \Sigma^2}\right) \exp\left[-\frac{v_{xy}^2 T^2}{4\Sigma^2}\right] \quad .$$

The above expression is accurate for large Σ. On the other hand, the most accurate representation for J for intermediate values of Σ is given by the integral in Eq. (B2). When the Rayleigh parameter is small ($\Sigma < 1$), the following series representation should be used

$$J = \left(\frac{4\pi^2 T^2}{\lambda^2}\right) e^{-\Sigma^2} \sum_{m=1}^\infty \left(\frac{\Sigma^{2m}}{m \cdot m!}\right) \exp\left[-v_{xy}^2 T^2/4m\right] \quad .$$

Section in [...] aspects, one analysis of a surface [...] distribution in surface heights has been considered. We will [...] corresponding expressions for J when the surface heights are distributed according to a bivariate exponential. Before the analysis for J as a function of Rayleigh parameter is presented, it is necessary to derive explicit expressions for the bivariate characteristic function and the univariate characteristic function for exponentially-distributed heights. The bivariate characteristic function for the exponentially-distributed surface heights is given by

$$
\chi_2 = \bar{c} \int_{-\infty}^{\infty} dZ_1 \int_{-\infty}^{\infty} dZ_2 \, \{\exp[i v_Z (Z_1 - Z_2)]\} \cdot
$$

$$
\cdot \left\{ \exp\left[- c_1 \left(\frac{Z_1^2 - 2c Z_1 Z_2 + Z_2^2}{(1 - c^2)} \right)^{1/2} \right] \right\} ,
$$

where

$$
\bar{c} = \frac{3}{2\pi\sigma^2(1 - c^2)^{1/2}}
$$

$$
c_1 = \sqrt{3}/\sigma \text{ , and}
$$

$$
v_Z = (2\pi/\lambda)(\cos\theta_i + \cos\theta_s) \ .
$$

To evaluate these integrals we first make the change of variables

$$
w = \frac{Z_1 - c Z_2}{\sqrt{1 - c^2}}
$$

and

$$
Z_1 = \sqrt{1 - c^2}\, w + c Z_2 \ .
$$

Then,

$$\chi_2 = \overline{c}\sqrt{1 - c^2} \int_{-\infty}^{\infty} dw \int_{-\infty}^{\infty} dZ_2 \left\{ \exp\left[iv_Z\left(\sqrt{1 - c^2}\, w + (c - 1)Z_2\right)\right]\right\} \cdot$$

$$\left\{ \exp\left[-c_1(w^2 + Z_2^2)^{1/2}\right]\right\}.$$

Next, we change to cylindrical coordinates, where $w = r \sin\theta$ and $Z_2 = r\cos\theta$, so that

$$\chi_2 = \overline{c}\sqrt{1 - c^2} \int_0^{\infty} r\, dr \int_0^{2\pi} d\theta\, e^{-iv_Z r[\sqrt{1-c^2}\sin\theta + (c-1)\cos\theta]}\, e^{-c_1 r}.$$

Performing the integration over r yields:

$$\chi_2 = \overline{c}\sqrt{1 - c^2} \int_0^{2\pi} d\theta\, \left[-c_1 + iv_Z\left(\sqrt{1 - c^2}\sin\theta + (c - 1)\cos\theta\right)\right]^{-2}.$$

This integral can be evaluated by the calculus of residues if we introduce the change of variables $Z = e^{i\theta}$, so the χ_2 becomes

$$\chi_2 = \frac{-4i\overline{c}\sqrt{1 - c^2}}{A^2}\oint \frac{Z\, dZ}{\left[Z^2 + (B/A)Z + (D/A)\right]^2}$$

where

$$A = v_Z\left[-i(1 - c) + \sqrt{1 - c^2}\right],$$

$$B = -2c_1,\quad \text{and}$$

$$D = v_Z\left[i(1 - c) + \sqrt{1 - c^2}\right],$$

and the contour is around the unit circle in the complex Z-plane. Cauchy's integral formula then leads to the result

$$\chi_2 = \left\{1 + (2/3)\Sigma^2[1 - c(\tau)]\right\}^{-3/2} .$$

An alternative derivation of this result was reported by Brown.[B4]

The marginal univariate density function corresponding to the bivariate exponential distribution is given by

$$p(Z_2) = 2\bar{c}\sqrt{1 - c^2} \int_{-\infty}^{\infty} du \, \exp\left[-c_1\left(u^2 + Z_2^2\right)^{1/2}\right]$$

$$= 2\bar{c}\sqrt{1 - c^2} \int_{Z_2}^{\infty} \frac{v \, dv \, e^{-c_1 v}}{\sqrt{v^2 - Z_2^2}} = 2\bar{c}\sqrt{1 - c^2} \, |Z_2| K_1(c_1|Z_2|) .$$

Then, the univariate characteristic function is given by

$$\chi = \int_{-\infty}^{\infty} p(Z_2) \, e^{iv_Z Z_c} \, dZ_2$$

and hence,

$$\chi = \left[1 + (1/3)\Sigma^2\right]^{-3/2} .$$

Here, it may be noted that $\chi_2(\tau \to \infty) \neq \chi \chi^*$ so that decorrelation does not imply statistical independence.

As in the Gaussian case, if the Rayleigh parameter is sufficiently large $(\Sigma \gg 1)$, then $\chi_2 - \chi\chi^* \approx \chi_2$ and the contributions to the four-fold integral [Eq. (1)] for J come primarily from the region where $\tau \approx 0$, so that

$$J = \left(\frac{4\pi}{\lambda^2}\right)\left(\frac{1}{A}\right) \int_{-X}^{X} dx_1 \int_{-X}^{X} dx_2 \int_{-Y}^{Y} dy_1 \int_{-Y}^{Y} dy_2 \left(\chi_2 \exp\left\{i\left[v_x(x_1 - x_2) + v_y(y_1 - y_2)\right]\right\}\right)$$

B4. Brown, G.S. (1982) Scattering from a class of randomly rough surfaces, Radio Sci. (to be published).

which reduces to

$$J \approx \left(\frac{8\pi^2}{\lambda^2}\right) \int_0^\infty J_0(v_{xy}\tau)\left[1 + (2/3)\Sigma^2\tau^2/T^2\right]^{-3/2}\tau\,d\tau \; .$$

This is the expression given by Barrick in Ruck et al.[B5]

On the other hand, if the Rayleigh parameter is not large ($\Sigma \le 1$, intermediate Rayleigh parameters), then

$$J = \left(\frac{4\pi}{\lambda^2}\right)\left(\frac{1}{A}\right) \int_{-X}^{X} dx_1 \int_{-X}^{X} dx_2 \int_{-Y}^{Y} dy_1 \int_{-Y}^{Y} dy_2 \; Q(x_1, x_2 y_1, y_2)[\chi_2 - \chi\chi^*] \; .$$

where

$$Q(x_1, x_2, y_1, y_2) = \exp\left[i(v_x[x_1 - x_2] + v_y[y_1 - y_2])\right] \; .$$

Brown[B4] has rewritten this expression as the sum of two integrals, by subtracting and adding the term

$$\chi_2(\tau \to \infty) = [1 + (2/3)\Sigma^2]^{-3/2} \; ,$$

which follows from $c(\tau \to \infty) = 0$. Then, $J = J_D + J_S$, where

$$J_D = \left(\frac{4\pi}{\lambda^2}\right)\left(\frac{1}{A}\right) \int_{-X}^{X} dx_1 \int_{-X}^{X} dx_2 \int_{-Y}^{Y} dy_1 \int_{-Y}^{Y} dy_2 \; Q(x_1, x_2, y_1, y_2)[\chi_2 - \chi_2(\tau \to \infty)]$$

and

$$J_S = \left(\frac{4\pi}{\lambda^2}\right)(4XY)\,\text{sinc}^2(v_xX)\,\text{sinc}^2(v_yY)\left[(1 + (2/3)\Sigma^2)^{-3/2} - (1 + (1/3)\Sigma^2)^{-3}\right] \; .$$

Here: $\text{sinc}(u) = \left(\frac{\sin u}{u}\right)$. Since most of the contribution to J_D comes from the region where $\tau \approx 0$, one may write

B5. Ruck, G. T., Barrick, D. E., Stuart, W. D., and Krichbaum, C. K. (1970)
Radar Cross Section Handbook, Vol. 2, Plenum Press, New York.

60

$$J_D = \left(\frac{4\pi}{\lambda^2}\right)(2\pi)\int_0^\infty J_0(v_{xy}\tau)\left[\left(1 + (2/3)\Sigma^2\{1 - c(\tau)\}\right)^{-3/2} - \right.$$

$$\left. \left(1 + (2/3)\Sigma^2\right)^{-3/2}\right]\tau\,d\tau \quad .$$

Brown[B4] has identified J_D as the incoherent-power scattered diffusely, and J_S as the incoherent power that is strongly peaked in the specular direction ($v_x = v_y \approx 0$).

If $\Sigma \ll 1$ (small Rayleigh parameter) then

$$\chi_2 \approx 1 - \Sigma^2 + \Sigma^2\,e^{-\tau^2/T^2}$$

and

$$\chi\chi^* \approx 1 - \Sigma^2$$

so that

$$(\chi_2 - \chi\chi^*) \approx \Sigma^2\,e^{-\tau^2/T^2}$$

and

$$J \approx \left(\frac{8\pi^2}{\lambda^2}\right)\Sigma^2\int_0^\infty J_0(v_{xy}\tau)\,e^{-\tau^2/T^2}\,\tau\,d\tau \quad .$$

Thus, for $\Sigma \ll 1$, (small Rayleigh parameter),

$$J \approx \left(\frac{4\pi^2}{\lambda^2}\right)\Sigma^2\,T^2\,\exp[-v_{xy}^2\,T^2/4] \quad .$$

We now have a series of expressions for the determination of the J term contribution to $\sigma°$. In Section 2, the accuracy of each of these expressions for J (and $\sigma°$) are investigated numerically for a wide range of Rayleigh parameters.

References

B1. DeSanto, J.A., and Shisha, O. (1974) Numerical solution of a singular integral equation in random rough surface scattering theory, J. Comp. Phys. 15(No. 2):286.

B2. Brown, G.S. (1982) New results on coherent scattering from randomly rough conducting surfaces, IEEE Trans. Antennas Propag. (to be published).

B3. Beckmann, P., and Spizzichino, A. (1963) The Scattering of Electromagnetic Waves From Rough Surfaces, Macmillan Co., New York.

B4. Brown, G.S. (1982) Scattering from a class of randomly rough surfaces, Radio Sci. (to be published).

B5. Ruck, G.T., Barrick, D.E., Stuart, W.D., and Krichbaum, C.K. (1970) Radar Cross Section Handbook, Vol. 2, Plenum Press, New York.

Appendix C

Differentiating Features of the Two Models

As was discussed in Appendix A, many of the details for the two models are identical. The point at which the models differ is in the calculation of the diffuse scattered power. In the discussion we will first present the specifics of the general model and then show how some simplifying assumptions lead to an alternative less complex formalism that includes the length and width definitions of Beckmann and Spizzichino.[C1] Ruck et al[C2] give expressions for the average bistatic rough-surface cross-section σ_o under the following four assumptions: (1) the radius of curvature of the surface irregularities is larger than a wavelength; (2) the roughness is isotropic in both surface dimensions; (3) the correlation length is smaller than either the X or Y dimension of the sample subregion; and (4) multiple scattering is neglected. The expression for σ_o has been presented in Appendix A. Here we wish to discuss the scattering matrix element that is used in the determination of the cross section of the rough surface.

The matrix elements for linear polarization states are

$$\beta_{VV} = \left(\frac{a_2 a_3 R_{\parallel}(\theta_i) + \sin \theta_i \sin \theta_s \sin^2 \phi_s R_{\perp}(\theta_i)}{a_1 a_4} \right)$$

C1. Beckmann, P., and Spizzichino, A. (1963) The Scattering of Electromagnetic Waves From Rough Surfaces, Macmillan Co., New York.

C2. Ruck, G. T., Barrick, D. E., Stuart, W. D., and Krichbaum, C. K. (1970) Radar Cross Section Handbook, Vol. 2, Plenum Press, New York.

$$\beta_{HV} = \sin \phi_s \left(\frac{-\sin \theta_i a_3 R_{\parallel}(\theta_i) + \sin \theta_s a_2 R_{\perp}(\theta_i)}{a_1 a_4} \right)$$

$$\beta_{VH} = \sin \phi_s \left(\frac{\sin \theta_s a_2 R_{\parallel}(\theta_i) - \sin \theta_i a_3 R_{\perp}(\theta_i)}{a_1 a_4} \right)$$

$$\beta_{HH} = \left(\frac{-\sin \theta_i \sin \theta_s \sin^2 \phi_s R_{\parallel}(\theta_i) - a_2 a_3 R_{\perp}(\theta_i)}{a_1 a_4} \right) .$$

Here, $R_{\parallel}(\theta_i)$ and $R_{\perp}(\theta_i)$ are the Fresnel reflection coefficients

$$R_{\parallel}(\theta_i) = \frac{\varepsilon_r \cos \theta_i - \sqrt{\varepsilon_r - \sin^2 \theta_i}}{\varepsilon_r \cos \theta_i + \sqrt{\varepsilon_r - \sin^2 \theta_i}}$$

and

$$R_{\perp}(\theta_i) = \frac{\cos \theta_i - \sqrt{\varepsilon_r - \sin^2 \theta_i}}{\cos \theta_i + \sqrt{\varepsilon_r - \sin^2 \theta_i}} .$$

Note that ε_r is the relative complex dielectric constant of the surface, the subscript $\parallel$ refers to the E-field in the plane of incidence, and the subscript $\perp$ refers to the E-field normal to the plane of incidence. The remaining angle terms are

$$\cos \theta_i = \frac{1}{\sqrt{2}} \sqrt{1 - \sin \theta_i \sin \theta_s \cos \phi_s + \cos \theta_i \cos \theta_s}$$

$$a_1 = 1 + \sin \theta_i \sin \theta_s \cos \phi_s - \cos \theta_i \cos \theta_s$$

$$a_2 = \cos \theta_i \sin \theta_s + \sin \theta_i \cos \theta_s \cos \phi_s$$

$$a_3 = \sin \theta_i \cos \theta_s + \cos \theta_i \sin \theta_s \cos \phi_s$$

$$a_4 = \cos \theta_i + \cos \theta_s .$$

Then, neglecting shadowing effects we have the general expression for the surface cross section

$$\sigma^\circ(\theta_i, \ \theta_s, \ \phi_s) = |\beta_{pq}|^2 J \quad .$$

The diffuse scattered power is determined by integrating the product of this expression and the corresponding elevation and azimuthal receiver and transmitter gain factors over the distance between the two antennas. The azimuthal integration is bounded by the extent of the azimuthal difference pattern, Figure 10. (For a discussion of the technique used to introduce these bounds into the formulation, see Papa, Lennon, and Taylor.[C3])

In the alternative model the assumption is made that the receiver is sufficiently far from the transmitter so that the portion of the "glistening surface" that contributes to the diffuse multipath is a long, narrow strip extending between the transmitter and receiver. This assumption allows us to make the approximation that the azimuthal scattering angle $\phi_s \approx 0^\circ$. This assumption leads to considerable change in the resultant σ° calculation.

In the scattering matrix, the first consideration is that the two cross-polarized terms are now zero. Only the copolarized elements contribute to the scattering. In those cases, manipulation of the relations and introducing the angle

$$\alpha = \left(\frac{\theta_i + \theta_s}{2} \right) \quad \text{leads to}$$

$$\beta_{VV} = \frac{(1 + \cos 2\alpha) R_{\parallel}(\theta_i)}{(\cos \theta_i + \cos \theta_s)} \qquad \text{(vertical polarization)}$$

and

$$\beta_{HH} = \frac{(1 + \cos 2\alpha) R_{\perp}(\theta_i)}{(\cos \theta_i + \cos \theta_s)} \qquad \text{(horizontal polarization)} \quad .$$

In these two terms it should be noted that each depends on only one Fresnel reflection component while in the general solution each includes contributions from the two Fresnel coefficients. Another effect of this assumption is seen in the terms ξ_x, ξ_y, and ξ_z. These reduce to $\xi_x = \sin \theta_i - \sin \theta_s$, $\xi_y = 0$, and $\xi_z = -\cos \theta_i - \cos \theta_s$. As a result we then have

C3. Papa, R.J., Lennon, J.F., and Taylor, R.L. (1980) Electromagnetic Wave Scattering From Rough Terrain, RADC-TR-80-300, AD A09839.

67

$$J = \left(\frac{T^2}{\sigma^2 \xi_z^2}\right) \exp\left[-\left(\frac{T^2}{4\sigma^2}\right)\left(\frac{\xi_x^2}{\xi_z^2}\right)\right]$$

for a Ga ;ian bivariate surface-height probability density function (PDF) and

$$J = \left(\frac{3T^2}{\sigma^2 \xi_z^2}\right) \exp\left[-\left(\frac{\sqrt{6}\,T}{2\sigma}\right)\left(\frac{\xi_x^2}{\xi_z^2}\right)^{1/2}\right]$$

for an exponential surface-height PDF.

Since this has effectively removed any azimuthal variation in σ°, the calculation of the diffuse power scattered by the surface and received at the antenna is approached differently. In this model, the surface of integration is determined by the Beckmann and Spizzichino definitions of glistening surface length and width. The length is obtained by calculating the location of the two end points of the glistening surface. For a homogeneous surface, the distances from the end points to the transmitter and receiver (L_1, L_2) are based on the respective heights (H_T, H_A) and a roughness criterion (σ/T), where σ^2 is the surface height variance and T is the correlation length. Then,

$$L_1 = H_T \cot(2\beta_o)$$

$$L_2 = H_A \cot(2\beta_o) \tag{C1}$$

where,

$$\tan \beta_o = 2\sigma/T \quad .$$

Then, along the extent of the surface the local width W is given by

$$W = \left(\frac{2X_1 X_2}{D}\right)\left(\frac{H_A}{X_1} + \frac{H_T}{X_2}\right)\left[\tan^2 \beta_o - 0.25 \left(\frac{H_A}{X_1} - \frac{H_T}{X_2}\right)^2\right]^{1/2} . \tag{C2}$$

Here,

D = total ground distance from transmitter to receiver,

X_1 = distance from transmitter to point on glistening surface, and

X_2 = distance from receiver to point on glistening surface.

Once these quantities have been determined, the diffuse scattered power contribution from each increment of length along the glistening surface is obtained by multiplying the product of the centerline value of σ° and W by the appropriate azimuthal and elevation plane antenna power-pattern distributions.

The differences in the various results described in Section 3 and Section 4 of this report reflect the effects of using the two alternative models in our analyses. One additional point that can be made is that in an earlier report[C4] we described an attempt to go beyond the Beckmann and Spizzichino model limits without resorting to the complete solution described here. In that instance, the restriction on the surface of integration based on the length of the glistening surface was removed and the calculation was made over the entire distance between antennas whether or not that exceeded the traditional glistening surface length. However, we still assumed $\phi_s \approx 0$ and the standard width values were used.

C4. Papa, R.J., Lennon, J.F., and Taylor, R.L., The Need For An Expanded Definition of Glistening Surface, RADC-TR-82-271.